The dual acting chemotherapeutic agent Alchemix induces cell death independently of ATM and p53.

Anoushka Thomas[‡], Tracey Perry[‡], Sarah Berhane[‡], Ceri Oldreive[‡], Anastasia Zlatanou[‡], Luke R Williams[‡], Victoria J. Weston[‡], Tatjana Stankovic[‡], Pamela Kearns[‡], Klaus Pors[§,1], Roger J Grand[‡,1], Grant S Stewart[‡,1]

[‡] IBR West Extension, School of Cancer Sciences, College of Medicine and Dentistry, University of Birmingham, Vincent Drive, Edgbaston, Birmingham, B15 2TT, UK,
[§] Institute of Cancer Therapeutics, School of Life Sciences, University of Bradford, West Yorkshire BD7 1DP, UK

[1] To whom correspondence should be addressed:

Tel: +44 121 414 9168 (GSS); +44 121 414 2805 (RJG); +44 1274 236482 (KP)
Email: G.S.Stewart@bham.ac.uk, R.J.A.Grand@bham.ac.uk or k.pors1@bradford.ac.uk.

Running title: Alchemix: a dual acting chemotherapeutic agent

Abstract

Topoisomerase inhibitors are in common use as chemotherapeutic agents although they can display reduced efficacy in chemotherapy-resistant tumours, which have inactivated DNA damage response genes, such as *ATM* and *TP53*. Here, we characterize the cellular response to the dual-acting agent, Alchemix (ALX), which is a modified anthraquinone that functions as a topoisomerase inhibitor as well as an alkylating agent. We show that ALX induces a robust DNA damage response at nano-molar concentrations and this is mediated primarily through ATR- and DNA-PK- but not ATM-dependent pathways, despite DNA double strand breaks being generated after prolonged exposure to the drug. Interestingly, exposure of epithelial tumour cell lines to ALX *in vitro* resulted in potent activation of the G2/M checkpoint, which after a prolonged arrest was bypassed allowing cells to progress into mitosis where they ultimately died by mitotic catastrophe. We also observed effective killing of lymphoid tumour cell lines *in vitro* following exposure to ALX, although, in contrast, this tended to occur via activation of a p53-independent apoptotic pathway. Lastly, we validate the effectiveness of ALX as a chemotherapeutic agent *in vivo* by demonstrating its ability to cause a significant reduction in tumour cell growth, irrespective of *TP53* status, using a mouse leukaemia xenograft model. Taken together, these data demonstrate that ALX, through its dual action as an alkylating agent and topoisomerase inhibitor, represents a novel anti-cancer agent that could be potentially used clinically to treat refractory or relapsed tumours, particularly those harbouring mutations in DNA damage response genes.

Keywords Alchemix, ATM, ATR, p53, DNA damage, apoptosis, mitotic catastrophe, replication stress, Chk1, T-ALL.

Introduction

Topoisomerase inhibitors are used as chemotherapeutic agents because of their potent ability to induce tumour cell death[1-4]. Typically, topoisomerase II (TOP2) inhibitors fall into two classes depending on their target[1,5]. The class I group (e.g. etoposide, doxorubicin, mitoxantrone) affects the catalytic activity of TOP2 during the DNA cleavage/ligation reaction resulting in stabilisation of the TOP2 cleavage complex in the presence of unligated DNA double strand breaks (DSBs), ultimately triggering apoptosis. The second class inhibits the catalytic activity of TOP2 before cleavage-complex formation and DSB generation and functions by reducing levels of chromosome-bound TOP2. As a consequence, since TOP2 is required to decatenate replicated DNA molecules before the onset of chromatid separation during mitosis, treatment with this type of TOP2 inhibitor (e.g. aclarubicin) induces cell death by mitotic catastrophe due to anaphase-associated fragmentation of catenated chromatids[6].

Whilst TOP2 inhibitors have been used relatively successfully as a mono-therapy, recently this approach has been largely superseded by combination therapies due to the ease with which tumour cells develop resistance[7]. Specifically, it has been shown that the acquisition of mutations in DNA damage response (DDR) genes, such as *ATM* and *TP53*, a reduction in the cellular pools of TOP2 protein or the over-expression of drug efflux pumps, are common underlying causes of tumours becoming refractory to TOP2 inhibitors[8]. Therefore, there is a clinical need for second-generation TOP2 inhibitors that can circumvent these mechanisms of drug resistance. Accordingly, a series of modified, anthraquinone-based compounds have been developed that combine the capability of class I TOP2 inhibitors to induce DSBs with the DNA damaging ability of alkylating agents[9-11]. The rationale for development of these multi-functional DNA damaging agents is that they should induce genetic damage to such an extent that it cannot be tolerated even in the presence of mutations that compromise specific DNA repair, checkpoint or apoptotic pathways. Of these compounds Alchemix (ALX) was demonstrated to have the most potent anti-tumour activity *in vivo* using a xenograft mouse model[9]. Furthermore, ALX was not affected by over-expression of the multi-drug resistance gene *P-gp* indicating that it may be a more effective chemotherapeutic agent for treatment of tumours that have developed resistance to non-covalent DNA binding anthraquinone-based drugs. Despite this, it is not known which DNA damage pathways are activated following ALX treatment and whether the inactivation of tumour suppressor genes that are important critical regulators of these pathways, such as *ATM* or *TP53,* could cause resistance. In this study we use a biochemical approach to determine the mode

of action of ALX to ascertain whether it could be potentially used clinically to treat tumours that have developed resistance to conventional chemotherapeutic agents.

Results

Alchemix induces a marked ATR-dependent DNA damage response in tumour cells, independently of ATM and p53.

To understand how ALX derives its potent anti-tumour activity we initially exposed HeLa cells to a range of concentrations of the drug and examined the activation of the DDR after 5 and 24 hours, using Western blotting, coupled with antibodies recognising known substrates of the PI-3-kinase-like kinases (PIKK), ATM and ATR. Phospho-ATM (S1981) was used a marker of ATM activation. Phospho-SMC1 (S966), Nbs1 (S343) and Chk1 (S345) were used as markers of cell cycle checkpoint activation. Lastly, phospho-RPA and γ-H2AX were used as markers of DNA damage. A dose of 10-100nM elicited a significant response; therefore, 50nM was used for most experiments (Fig. S1A, S1B). To confirm these observations and to determine whether p53 status affected the cellular response to ALX, several cancer lines (described in Table S1) were treated with ALX (50nM) and the activation of DDR pathways was monitored. Whilst the kinetics of DNA damage-induced signalling varied somewhat between the individual cell lines, we repeatedly observed strong activation of the DDR suggesting that the anti-tumour activity of ALX is probably mediated through its ability to induce DNA damage (Fig.1A, 1B, 1C, S1C, S1D).

Unlike other anthraquinone-based drugs, such as doxorubicin and mitoxantrone, which induce DNA damage by inhibiting TOP2, ALX can also damage cellular DNA through its alkylating side chain[10]. To determine which activity of ALX is more important for activating the DDR, we exposed HeLa cells to ALX or a derivative (ZP275) that cannot alkylate DNA whilst retaining its ability to inhibit TOP2. Whereas both compounds could induce phosphorylation of known PIKK substrates, loss of the alkylating side chain severely attenuated the DDR, indicating that it is a combination of these two DNA damaging properties that is important for ALX activity (Fig.1C). Moreover, ALX treatment failed to induce the mono-ubiquitylation of PCNA, typically observed in cells exposed to compounds that alkylate DNA or agents that induce replication fork stalling (Fig.S2). This suggests that the mechanism underlying the DNA alkylation activity of ALX occurs in a manner distinct from other chemotherapeutics.

In contrast to the signalling induced by ionising radiation (IR) or UV, the relative contribution of the individual PIKKs to activation of specific DDR pathways following exposure to class 1 TOP2 inhibitors is less well understood. It has been previously reported that both ATM and ATR are activated in cells exposed to the TOP2 inhibitors etoposide or doxorubicin[12,13]. This is clinically important since *ATM* is commonly mutated in many tumour types. One potential

underlying reason for this is that these agents can induce both DNA DSBs as well as stalled replication forks, which activate ATM and ATR, respectively.

To ascertain whether ALX was capable of inducing DNA DSBs and activating an ATM-dependent DDR, HeLa cells were treated with ALX over 24 hours. Cells were fixed and immunofluorescence microscopy used to monitor DSB formation. Despite H2AX being strongly phosphorylated early in response to ALX treatment (2h), only at later times (8-24h) were γ-H2AX/53BP1 foci discernible, indicating that DSBs are only formed after prolonged exposure (Fig.2A, 2B). This observation was supported by carrying out pulse-field gel electrophoresis on these cells following exposure to varying doses of ALX (Fig.2C). However, from our preliminary analysis of the DDR induced by ALX in tumour cell lines, the low level of ATM S^{1981}auto-phosphorylation suggested that, despite the ability of ALX to generate DSBs, ATM is not markedly activated (Fig. 1A, 1B). This is supported by the observation that ALX did not induce the phosphorylation of KAP1 or Chk2, two specific substrates of ATM (Fig.S3A). Furthermore, combining the ATM inhibitor with ALX did not significantly affect activation of the DDR (Fig.S3B, S4A, S4B, S4C).

Since TOP2 inhibitors also induce replication-associated DNA damage, this would suggest that ATR could play a role in activating the damage-induced signalling pathways. To determine the contribution of ATR, DLD1 cells, engineered to mimic the human Seckel Syndrome-associated hypomorphic *ATR* mutation and its *ATR* complemented counterpart (Fig.3A), were exposed to ALX and the DDR monitored. Consistent with a role for ATR in controlling the DNA damage response to ALX, compromising the level of ATR reduced phosphorylation of several DNA damage-regulated repair/checkpoint proteins; this was rescued by re-expression of ATR (Fig.3A). Consistent with this, depletion of Claspin, a protein required for ATR-dependent Chk1 activation, reduced ATR-dependent phosphorylation of Chk1, induced by ALX (Fig.S5). These observations indicate that, unlike other DNA intercalating TOP2 inhibitors, ALX primarily elicits an ATR- but not ATM-dependent DDR, despite inducing DSBs.

Interestingly, the phosphorylation of H2AX and RPA2 in DLD1-Seckel cells was highly elevated following ALX treatment, compared to the complemented cells (Fig.3A). Whilst ATR phosphorylates H2AX following exposure of cells to agents that stall replication forks[14], it is likely that the observed enhanced phosphorylation of H2AX signifies the induction of replication stress, DSB formation and activation of a redundant PIKK. Consistent with this, knock-in DLD1 cells in which an activation-associated serine residue of Chk1 was mutated to alanine (S317A) exhibited a similarly exacerbated phosphorylation of H2AX/RPA2 response following exposure

to ALX (Fig.3B). This indicates that the ATR-Chk1 checkpoint pathway is not only required to signal activation of the DNA damage-induced intra-S phase checkpoint, but is also essential for stalled replication fork stability. Treatment of DLD1-Seckel cells with ALX and an ATM inhibitor did not alleviate the induced replication stress, suggesting that in the absence of ATR, ATM is playing only a minor role in signalling pathways induced following ALX-dependent replication fork collapse (Fig.3D, S6A). Based on this, it is likely that DNA-PK, which normally regulates repair of DSBs by NHEJ, also responds to DSBs induced during replication stress. It has been previously reported that DNA-PK undergoes auto-phosphorylation after the treatment of cells with genotoxic agents such as UV, hydroxyurea and the TOP1 inhibitor, camptothecin[15,16]. In addition, DNA-PK becomes rapidly activated following nucleotide depletion when Chk1 activity is compromised[17]. Consistent with this, we observed increasing DNA-PK activation following exposure of HeLa cells to ALX, suggesting that it may be involved in regulating the cellular response to this DNA damaging agent (Fig.3C). To determine whether DNA-PK was responsible for the elevated phosphorylation of H2AX and RPA in ALX-treated DLD1-Seckel cells, we exposed these cells to ALX in the presence or absence of a DNA-PK inhibitor (Fig.3D). Strikingly, we observed that the H2AX and RPA2 phosphorylation induced by ALX in these cells was completely suppressed by the DNA-PK inhibitor, indicating that DNA-PK functions redundantly with ATR (Fig.3D). Surprisingly, we observed a modest reduction in the phosphorylation of Nbs1, Chk1 and RPA2 in cells treated with ALX and the DNA-PK inhibitor (Fig.S6B), indicating that DNA-PK may also play a role in activating the cell cycle checkpoint pathway rather than just responding to replication-associated DSBs.

Taken together these data demonstrate that Alchemix induces a DNA damage response primarily mediated by ATR and DNA-PK, which requires its ability to inhibit the TOP2 cleavage complex and to alkylate DNA.

Alchemix requires both TOP2α and TOP2β to elicit a DNA damage response but not mismatch, Fanconi Anaemia or ubiquitin-dependent repair pathways.

To investigate which components of the damage response machinery, besides the ATR-Claspin-Chk1 replication-stress pathway, were important for eliciting a DDR following exposure to ALX, siRNA and knockout cell lines were used. To ascertain if the DNA damage, particularly the DSBs, generated during ALX treatment largely depends on the presence of TOP2, cells were transfected with TOP2α or TOP2β directed siRNAs, exposed to ALX and the DDR examined (Fig.4). Loss of either TOP2α or TOP2β alone failed to alleviate ALX-induced DNA DSBs,

suggesting that ALX is probably capable of inhibiting multiple class II topoisomerases, not just TOP2α (Fig.4) as reported previously[9]. Consistent with this, siRNA-mediated knockdown of both TOP2α and TOP2β reduced ALX-induced RPA2 phosphorylation (and that of H2AX to a limited extent), indicating that ALX is capable of targeting both forms of TOP2 *in vivo* (Fig.4). However, knock down of TOP2α and/or TOP2β resulted in an elevated ATR-dependent checkpoint response following ALX treatment (Fig.4), suggesting that events, independent of TOP2 inhibition, cause DNA lesions that largely determine its capacity to stall replication forks and activate ATR.

The mismatch repair (MMR) pathway plays a key role in the response to DNA alkylating agents and is essential for activation of the ATR checkpoint pathway[18,19]. As the ability of ALX to activate the ATR-dependent DDR requires its capacity to alkylate DNA, it is conceivable that this requires the MMR pathway. However, depletion of MSH2, critical to the MMR machinery, exacerbated rather than reduced the ALX-induced cellular DDR, demonstrating that the MMR pathway is dispensable for ALX-induced ATR activation (Fig.S7A). This suggests that tumour cells with deficiencies in MMR could be hypersensitive to the killing effects of ALX as previously observed for other structurally related anthraquinone-based agents[20,21].

To ascertain if the Fanconi Anaemia (FA) and the RNF8-dependent ubiquitin-dependent repair pathways[21], were involved in co-ordinating the cellular response to ALX, cells with or without FANCF or depleted of RNF8 were exposed to ALX and the damage response determined. Compromising either the FA repair machinery or RNF8-dependent DNA damage-induced ubiquitylation affected the ALX-induced DDR significantly, suggesting that loss of these tumour suppressor pathways is unlikely to cause ALX resistance (Fig.S7B, S7C).

Exposure to low dose ALX leads to G2/M checkpoint arrest, checkpoint slippage-associated mitotic abnormalities and death by mitotic catastrophe.

Since TOP2 is critically involved in removing DNA supercoils resulting from DNA unwinding during replication and separating catenated sister chromatids prior to the onset of anaphase, it is likely that treating cells with ALX will have detrimental effects on progress through both S-phase and mitosis. To determine how the kinetics of the DDR correlated with transit through the cell cycle, HeLa cells were exposed to a low dose of ALX and samples analysed by FACS analysis. Consistent with the early activation of ATR-dependent checkpoint response, cells treated with ALX for 4-8h accumulated in S-phase (Fig.5A). In keeping with the late induction of DSBs and subsequent activation of a DNA-PK-dependent DDR, cells treated

with ALX for 24h accumulated in late-S/G2-phase of the cell cycle as judged by the elevated levels of Cyclins A/B and low levels of phosphorylated histone H3 (Fig.5A, 5B). However interestingly, a significant proportion of the cells bypassed the checkpoint and progressed into mitosis with unrepaired DNA damage, which resulted in the development of severe mitotic abnormalities, such as misaligned/fragmented chromosomes, anaphase-bridging and multi-polar spindles (Fig.5C).

To determine whether the accumulation of DNA damage in cells entering mitosis contributes to cell death, HeLa cells were treated with higher doses of ALX and harvested every 24h for analysis by FACS, Western blotting and immunofluorescence microscopy. As a control, cells were also treated with cisplatin to induce cell death through classical apoptotic pathways. As expected, cisplatin induced cell death predominantly by apoptosis, seen as by PARP1 and Lamin B1 cleavage, proteolysis (activation) of Pro-caspase 3 and nuclear fragmentation (Fig.6A, 6B). In contrast, although higher concentrations (up to 0.5μM) of ALX could induce a significant amount of cell death (Fig.6A), this was not associated with markers of apoptosis or autophagy, (Fig.6B, S8A), suggesting that these are not a major mode of cell death at these doses. A similar response was also seen in the p53 *wt* U2OS cell line as well as the p53-null H1299 cell line (Fig.S8B, S8C). However, it should be noted that PARP1 was consistently observed to be cleaved to a limited extent at early times in some cell lines following ALX exposure (Fig.6B). Despite this, we observed that ALX primarily induced cell death through a mechanism consistent with mitotic catastrophe/abortive mitosis, although a small proportion of the ALX-treated cells underwent apoptosis (Fig.6C, 6D). Interestingly, cells undergoing prolonged mitotic arrest can trigger a partial apoptotic response and induce p53, following slippage into the next G1 phase of the cell cycle[23]. In this respect, exposure to ALX can lead to the stabilisation of p53, although its ability to up-regulate downstream transcriptional targets, such as HDM2 and p21, appeared to be limited to later time following drug treatment, which coincided with the formation of DSBs and the appearance of abnormal mitotic cells (Fig.S8D). This could in part explain the apoptotic-like cell death we observed in cells expressing *wt* p53 following exposure to very high doses (>1μM) of ALX (Fig.7C, S9C).

Induction of DNA damage and cell death following exposure to ALX is enhanced in cycling cells and can be exacerbated under conditions of replication stress.

Given that the primary DDR response following ALX treatment requires ATR and that ALX-induced loss of cell viability is predominantly mediated through mitotic catastrophe, this suggests that cycling cells would be predicted to be more responsive to ALX. To test this,

hTERT-immortalised RPE1 cells were synchronised in G0/G1 by serum starvation or left to cycle asynchronously, treated with ALX and the DDR examined. Consistent with a cell cycle-dependency for ALX to induce a DDR, cells arrested in G0/G1 exhibited a highly attenuated ATR-dependent DNA damage response, with the expression of a number of the key regulatory effector molecules, such as Chk1, being down-regulated (Fig.7A). Consequently the arrested cells demonstrated an increased resistance to killing effects of ALX (Fig.7B, 7C). Again, as noted above, only at very high doses of ALX was cleavage of PARP1 and Lamin B1 observed.

It has been previously shown that pre-malignant cells commonly exhibit uncontrolled DNA replication that gives rise to elevated levels of DNA damage, which needs to be bypassed before a tumour can progress. This has been termed 'replication stress'. Whilst a number of genetic and epigenetic factors have been implicated in inducing replication stress, the most closely studied of these is the activation of certain oncogenes. Over-expression of Cyclin E, commonly associated with many tumours, causes an increase in replication fork stalling and DSBs[24,25]. Since this hallmark of pre-malignant cells mildly mimics the cellular response to ALX we considered whether treatment of replication-stressed cells with ALX may exacerbate the cellular DDR. U2OS cells with either normal or significantly elevated levels of Cyclin E were exposed to ALX and the DDR monitored. Cells over-expressing Cyclin E exhibited an increased DDR, particularly the phosphorylation of RPA2 and H2AX, which coincided with the earlier generation of DSBs as judged by 53BP1 foci formation (Fig.8A, 8B). A similar exacerbation of the DDR was also observed when immortalised human fibroblasts were infected with a recombinant adenovirus expressing Cyclin E or induced to over-express mutant H-Ras^{G12V} and then exposed to ALX (Fig.S9A, S9B). Moreover, the increased replication stress induced by Cyclin E over-expression in U2OS cells resulted in an earlier onset of an apoptotic-like cell death following exposure to a very high dose of ALX (Fig.S9C). This supports the idea that ALX may have some specificity towards tumour cells with deregulated DNA replication and high levels of replication stress.

ALX exhibits therapeutic potential against lymphoid tumours irrespective of *TP53* status *in vitro* and *in vivo*.

Resistance to treatment is a feature of subsets of most tumour types and, in the case of lymphoid tumours, such as B and T cell ALL, is frequently associated with mutations in DDR genes such as *ATM* and *TP53* or the up-regulation of multi-drug resistance gene expression[26-28]. While chemo-resistance is evident in some treatment-naive tumours, genetic changes associated

with chemotherapy resistance are frequently acquired during prolonged exposure to cytotoxic agents[29,30]. In ALL, around 10% of paediatric patients and over 50% of adult patients fail to undergo complete remission or experience relapse following treatment. As mutations in *TP53* play a major role in high risk and relapsed ALL disease[30-32] ALX might represent a useful therapeutic approach for these tumours**.** To investigate this, we tested the efficacy of ALX *in vivo* against primary and immortalised tumour cells with different p53 status (Fig.9A). These included a primary paediatric T-ALL sample (BCH-505) and the Molt4 T-ALL cell line, both of which have *wt TP53*, and the *TP53* mutant T-ALL cell lines CCRF-CEM and Jurkat. The primary T-ALL BCH-505 was engrafted into NOG mice, such that cells disseminated to the lymphoid organs within 4 weeks. The T-ALL tumour cell lines were injected subcutaneously to enable analysis of visible tumours. Following two doses of ALX, we observed a marked reduction in subcutaneous tumour size for the cell lines as well as the spleen weights (an indicator of tumour engraftment) and human CD45 tumour load in the primary T-ALL BCH-505 treated animals (Fig.9B, 9C). This indicates no apparent difference in the sensitivities of the *TP53 wt* and mutant tumours to ALX *in vivo*.

To confirm the mechanism of killing, Western blotting was employed to establish that ALX induced a DDR in the T-ALL cell lines (Fig.9A). Significant cell death was observed in all ALL cell lines in response to low dose ALX (summarized in Table S2) with considerable activation of apoptotic pathways as judged by the rapid cleavage of PARP1, LaminB1 and Pro-caspase 3 in (Fig.S10). This indicates that ALX can induce tumour cell death through multiple different pathways depending on the cell type treated and the dose used.

Discussion

Most current empirically-based chemotherapeutic agents kill tumour cells by inducing irreparable genomic damage, leading to apoptosis. However, even complex and intensive combinations of cytotoxic agents fail to overcome the evolution and selection of treatment-induced sub-clones in some tumours, which leads to the outgrowth of refractory disease[29,30,34,35]. Such sub-clones frequently arise following mutations in mediators of DNA damage-induced cell death, such as TP53. One major problem in combating treatment resistance is that our understanding of the mechanism of action of many chemotherapeutic agents currently used is limited.

Here we demonstrate that ALX can induce a two-stage DNA damage response that requires its ability to inhibit TOP2 and to alkylate DNA. Treatment of tumour lines with ALX induces replication damage, which in turn activates an ATR-dependent DDR and culminates in cells accumulating in G2-phase. It is likely that enzymatic processing or spontaneous collapse of stalled/aberrant replication forks results in the generation of DNA DSBs that triggers DNA-PK activation (summarized in Fig.10). This DDR can be initiated in the absence of known tumour suppressor genes, such as *ATM*, *TP53*, *FANCF* and *MSH2*, the mutation of which have been associated with treatment resistance. Moreover, despite a requirement for ATR and Chk1 to mediate activation of the ALX-induced cell cycle checkpoint, loss of this pathway exacerbates the formation of DSBs, indicating a role for ATR in preventing stalled replication fork collapse caused by exposure to ALX.

The DNA damage induced by ALX requires the presence of TOP2. However, in contrast to previously published data indicating that ALX specifically inhibits TOP2α, the depletion of both TOP2 isoforms was required to reduce ALX-induced phosphorylation of H2AX. Based on this observation, it is conceivable that resistance to ALX could develop by reducing cellular pools of TOP2α and β. Interestingly however, depletion of TOP2α and β does not affect activation of the ATR-dependent checkpoint response following exposure to ALX, indicating that suppression of cell replication and division could still be achieved with reduced TOP2 expression. Therefore, it is tempting to speculate that this is dependent upon its DNA alkylation function, which we have demonstrated is important for the ability of ALX to induce a DDR.

Given the complex nature of ALX's ability to produce a variety of different deleterious DNA lesions, it is unsurprising that the mechanisms by which it induces cell death are complicated. Despite ALX treatment causing cell cycle arrest in S and G2 phases of the cycle, it is clear that checkpoint slippage can occur and cells enter mitosis, most probably with unrepaired DNA DSBs, under-replicated DNA and/or catenated sister chromatids. As a result a major cause

of cell death in epithelial tumour lines is through mitotic catastrophe after treatment with low doses of ALX. On this basis, since mitotic catastrophe does not require a functional ATM-p53 axis, tumour cells normally resistant to most conventional chemotherapeutic agents, due to mutations in this pathway, should be sensitive to killing by ALX. However, we did observe that ALX, at low dose, could induce apoptosis in HeLa cells, albeit to a low level, as judged by the partial PARP1 cleavage. Although it should be noted that this did not coincide with Pro-caspase 3 nor Lamin B1 cleavage indicating the possible activation of a non-canonical apoptotic pathway. In this respect, it has been observed that cells undergoing a prolonged block in mitosis can induce a p53-dependent apoptotic mode of cell death following slippage into the subsequent G1 phase of the cell cycle[23]. Consistent with this, we observed that ALX can induce the stabilisation of p53, although it only appeared to be transcriptionally competent at later times during the DDR, probably linked with the generation of DSBs. It is therefore conceivable that ALX can induce cell death through either mitotic catastrophe and/or apoptosis. In keeping with this, ALX robustly induces apoptosis in the lymphoid tumour cells although this did not appear to require p53. Taken together our observations indicate that ALX can induce cell death through multiple different pathways in a variety of cell types independently of key regulators of the DDR known to be associated with treatment resistance.

Since *ATM* and *TP53* are commonly mutated in lymphoid tumours and this is associated with increased disease progression and treatment resistance, to ascertain whether ALX could be used as an effective chemotherapeutic agent *in vivo* to target these tumours we used T-ALL xenografts as a model for treating lymphoid tumour cells with and without *TP53* mutations. *In vitro*, ALX was able to induce a robust DDR and a significant amount of cell death in all three T-ALL tumour cell lines to a similar degree irrespective of *TP53* status. Consistent with this, we observed that ALX was able to significantly reduce the tumour load in mice engrafted with any of three T-ALL cell lines tested. Moreover, similar observations were seen in mice engrafted with a patient-derived, primary T-ALL tumour.

In summary, we propose that ALX, through its ability to activate different pathways of the DDR and to induce cell death by mitotic catastrophe and/or apoptosis, represents a novel therapeutic agent with a clinical potential to treat resistant/relapsed tumours harbouring mutations in DDR genes.

Materials and Methods

Cell lines

The human cell lines used in this study are detailed in Supplementary Table S1.

Drug treatments

Alchemix[9] and ZP275 were dissolved in DMSO and routinely added to cells to give a final concentration of 50nM in the culture medium. For experiments examining cell killing, ALX concentrations of 150 and 500nM were used. Cisplatin (EBEWE Pharma) was used at a concentration of 10μg/ml. The ATM inhibitors, KU-55933 (Merck) or KU60019 (Tocris) were used at 10μM, the DNA-PK inhibitor, NU7441 (Tocris) was used at 10μM and the ATR inhibitor, VE-821 (Selleckchem) was used at 5μM. 4-hydroxy-tamoxifen (Sigma) was used at 334nM.

siRNA treatment.

Smart-pools (Thermo) of siRNA were used to reduce expression of MSH2, Mre11, TOP2α and TOP2β. siRNA (0.4nmoles) was transfected into cells ($4x10^5$) using Oligofectamine (Invitrogen). Experiments were performed 72 hours later.

Quantification of autophagy

HEK293A cells, expressing GFP-LC3[33] were cultured in DMEM/10% FCS and this served as full media. Earle's balanced salt solution (EBSS) was starvation medium. 293/GFP-LC3 cells were seeded onto glass coverslips, 24h later full media was replenished in the presence or absence of ALX and the cells left for 24h. Starvation was induced in EBSS for the final 4 hours where indicated. Cells were fixed with paraformaldehyde and mounted on glass slides. Multiple random fields were collected and GFP-LC3-labelled structures counted.

Western blotting and antibodies.

Cell pellets were solubilized in 9M urea, 50mM Tris HCl pH7.4, 0.15M β mercapto-ethanol and proteins extracted before being fractionated on polyacrylamide gels run in 0.1M Bicine, 0.1M Tris, 0.1% SDS. Antibodies used in this study are listed in Supplementary Table S3.

FACS analysis.

FACS analysis was used to determine the percentage of dead cells after drug treatments. Cells were harvested and stored in 70% ethanol at -20°C. They were then suspended in propidium iodide (25µg/ml), RNAse (0.1mg/ml) at 37°C. DNA profiles were obtained using either an XL-MCL or Accuri flow cytometer. Proportions of cells in different phases of the cell cycle were calculated using WinMDI version 2.9.

Immunofluorescence microscopy.

Immunofluorescence was carried out as previously described[36].

Pulse-field Gel Electrophoresis (PFGE)

PFGE was carried out as previously described[37].

In vivo xenograft models: lymphocytic leukaemia

All procedures complied with U.K. home office guidelines. Primary leukemic material was obtained with ethical consent from Birmingham Children's Hospital (CCLG 08/H0405/22, 08/H1208/4 and 09/H1010/75). The T-ALL cell lines, Jurkat, CEM and Molt4, were injected subcutaneously into the flanks of NOG mice ($3x10^6$ cells/mouse). When tumours became palpable in ≥65% of mice, animals were randomized into two groups (n=6 per group). Two weekly doses of ALX (8mg/kg) were administered via intra-peritoneal (IP) injection (days 0 and 7) following initiation of treatment to the test group while the control group received 'vehicle' (1% DMSO/PBS) alone. During treatment tumour volumes were determined for up to 16 days or until the control tumours reached the maximum permitted volume. For the primary T-ALL sample (BCH-505), $1x10^6$ cells/mouse were injected via the lateral tail vein into NOG mice and the peripheral blood sampled weekly and stained using anti-human CD45 antibody. When the percentage of human CD45 cells in the blood reached ≥1%, mice were randomized into two groups (n=6/group) and received either two single weekly doses of ALX (8mg/kg) or 'vehicle'. When the proportion of human CD45 cells reached ≥25% in the blood in the control group, animals were sacrificed. Harvested spleens were weighed. Single cell suspensions were obtained from the spleens and bone marrow and stained for the presence of human CD45 to determine the final human tumour load.

Acknowledgments.

We are most grateful to Fred Bunz, Alan D'Andrea, Eva Petermann, Panagiotis Kotsantis and Jiri Lukas for the gift of cell lines and Philip Byrd, Arnold Levine and David Lane for antibodies. We would especially like to thank Cyrus Vaziri for providing cell lines and a recombinant adenovirus expressing Cyclin E, Rebbeca Jones for helping us with PGFE and Malcolm Taylor for helpful discussions. Lastly, we would also thank the University of Birmingham (AT - PhD studentship), MRC (GSS, RJG - Project grant: G0900088), Cancer Research UK (GSS - Senior Fellowship: C17183/A13030), Leukaemia Lymphoma Research (TS, GSS - Program grant: 11045), the Lister Institute (GSS, AZ - Research Prize) and Yorkshire Cancer Research (KP) for funding this study.

Figure legends.

Figure 1. ALX induces a DNA damage response in tumour cell lines. U2OS (A), H1299 (B) and HeLa (C) cells were treated with ALX (50nM) and harvested at the times shown. Protein phosphorylation was visualised by Western blotting using the antibodies shown. HeLa cells (C) were also treated with the ALX derivative, ZP275, which fails to alkylate DNA, as shown.

Figure 2. DNA double strand breaks are generated only after prolonged exposure to ALX. (A), HeLa cells were exposed to ALX and processed for immunofluorescence microscopy at the indicated times post-treatment. Cells were stained for γH2AX and 53BP1. Nuclear DNA was visualized with DAPI. (B), the proportion of γH2AX and 53BP1 foci (of various dimensions and intensities) formed was estimated on the basis of the representative images shown in the right-hand panel. The relative percentage of cells in each category at 24 hours after ALX treatment is shown in the left-hand panel. The type V γ-H2AX/53BP1 staining pattern is typical of undamaged cells in S-phase. (C), Pulse-field gel electrophoresis was used to detect the presence of DNA double strand breaks (DSBs) in cells that were treated with increasing concentrations of ALX for 24h. As a positive control for the presence of DSBs, cells were irradiated with 30Gy of ionising radiation (IR) and harvested 2h post-irradiation.

Figure 3. ALX induces a DNA damage response mediated by ATR and DNA-PK. (A), DLD1-Seckel cells and DLD1-Seckel cells complemented with ATR were exposed to ALX (50nM). Cells were harvested at the times shown. Protein phosphorylation was determined by Western blotting using the antibodies shown. (B), as (A) except that DLD1 cells in which Chk1 S^{317} had been mutated to alanine were used. (C), HeLa cells were treated with ALX for the times shown. The phosphorylation of DNA-PK_{cs} S^{2056} was determined by Western blotting. (D), DLD1-Seckel cells were treated with ALX for the times shown in the presence and absence of either the ATM inhibitor, KU60019, (10μM) or DNA-PK inhibitor, NU7441, (10μM). Protein phosphorylation was determined by Western blotting using the antibodies shown.

Figure 4. TOP2α and TOP2β are necessary for an ALX-induced DNA damage response. HeLa cells were depleted of TOP2α and/or TOP2β with siRNA and then exposed to ALX (50nM) for the times shown. Protein expression and level of protein phosphorylation were determined by Western blotting as shown.

Figure 5. Cells bypassing the ALX-induced G2/M checkpoint exhibit mitotic abnormalities. (A), HeLa cells were treated with ALX (50nM) and analysed by FACS. Cell cycle profiles obtained up to 24 hours are shown, together with the percentage of cells in the different stages of the cycle (inset). (B), HeLa cells treated with ALX (50nM) for 24 hours were Western blotted for the proteins shown. (C), HeLa cells were treated with ALX (50nM) for 24 hours and then examined by immunofluorescence microscopy. The number of cells in different stages of mitosis as well as those exhibit mitotic abnormalities was determined (left-hand panel). The percentage of cells with different mitotic abnormalities was determined (central panel). A minimum of 500 mitotic cells were counted per experiment. Examples of mitotic abnormalities seen in ALX-treated cells are shown in the right-hand panel.

Figure 6. Low dose ALX induces cell death in epithelial cells primarily by mitotic catastrophe and not by apoptosis. (A), HeLa cells were treated with ALX (500nM) or cisplatin (10μg/ml) for the times shown and then analysed by FACS. The percentage of cells in each stage of the cell cycle and in the sub-G1 population (taken as dead cells) is inset. (B), HeLa cells were treated with ALX (150nM or 500nM) or cisplatin (10μg/ml) for the times shown. After harvesting, lysates were Western blotted for PARP1, Lamin B1 and Pro-caspase 3. (C), HeLa cells were seeded on microscope slides and treated with ALX (150nM) or cisplatin (5μg/ml) for 24 hours. Cells were processed for immunofluorescence microscopy using antibodies against histone H3 phospho-serine S10, γH2AX, and Lamin B1. Nuclear DNA was stained with DAPI. Representative images showing staining in cells typical of apoptosis or mitotic catastrophe are presented. The percentage of cells undergoing each form of cell death is shown graphically in (D). A minimum of 500 mitotic cells were counted per experiment.

Figure 7. Non-cycling cells have a significantly reduced ALX-induced DNA damage response compared to their cycling counterparts. hTERT immortalised RPE1 cells were either arrested in G0/G1 by serum starvation or left to cycle asynchronously. (A), Cells were treated with ALX (50nM) as shown and subjected to Western blotting using the antibodies shown (upper panel). FACS analysis of the asynchronous and synchronised RPE1 cells in the absence of ALX treatment is shown in the lower panel. (B), Cycling and non-cycling RPE1 cells were treated with ALX (150nM or 500nM) or cisplatin (10μg/ml) for 48 hours. They were then analysed by FACS and the sub G1 peak taken as dead cells. (C), Cycling and non-cycling RPE1 cells were treated with ALX (1μM or 3μM) or cisplatin (30μg/ml). Cells were harvested at the times shown and Western blotted with antibodies against PARP1, Pro-caspase3, Lamin B1 and p53.

Figure 8. Replication stress enhances the ALX-induced DNA damage response. (A), U2OS cells with normal (+Tetracycline) or elevated expression of Cyclin E (-Tetracycline) were treated with ALX (50nM). Cells were harvested and protein expression determined by Western blotting using the antibodies shown. (B), U2OS cells, with normal or elevated expression of Cyclin E, were treated with ALX (50nM) for the times shown and processed for immunofluorescence microscopy. Upper panel shows cells stained with antibodies against γH2AX and 53BP1. Nuclear DNA was stained with DAPI. The lower panels show the percentage of cells with greater or less than five 53BP1 foci per cell.

Figure 9. The effect of ALX on leukaemic cells *in vitro* and *in vivo*. (A), ALX induces a DNA damage response in T-ALL cell lines, Jurkat, CEM and MOLT4 cells were treated with ALX (50nM) and harvested at the times shown. Western blotting of lysates with the antibodies shown was used to visualize protein phosphorylation. (B), ALX reduces the tumour load in mice with tumours derived from T-ALL cell lines. Cells were injected into NOG mice, which were then treated (as indicated by arrows) with vehicle or ALX (5mg/kg) as described. Tumour volume was measured. (C), ALX reduces tumour load in mice engrafted with paediatric T-ALL cells, BCH-505. The histograms show the relative size of the spleens in mice treated with ALX or controls at the time of death as well as the expression of human CD45 (*, $p \leq 0.05$; **, $p \leq 0.005$, ***, $p \leq 0.0005$).

Figure 10. A possible mechanism for the mode of action of ALX.

ALX inhibits TOP2 complexes present at a replication fork that results in the generation of a DNA double strand break (DSB). The binding of ALX to TOP2 may promote its ability to alkylate DNA in close proximity to a replication fork. The combination of a DSB and localised DNA alkylation is likely to result in fork stalling and activation of the ATR-dependent cell cycle checkpoint pathway. Following a prolonged growth arrest, a significant proportion of cells bypass the checkpoint and either enter into mitosis with unrepaired DNA damage that triggers mitotic catastrophe or activate p53-independent apoptosis. In cells lacking an intact ATR-Chk1 pathway or undergoing replication stress, an increased number of stalled/damaged replication forks collapse resulting in the activation DNA-PK. It is possible that attempted repair of a collapsed replication fork or TOP2-associated DSB by DNA-PK-dependent repair pathways produces deleterious DNA structures that exacerbate abortive mitosis.

Legends to supplementary figures.

Figure S1. Increasing concentrations of ALX induces an increased DNA damage response. Increasing concentrations of ALX were added to H1299 cells, which were harvested after 5 hours (A) and 24 hours (B). The concentrations of ALX used are shown at the top of the figure. (C), DLD-1 cells were treated with ALX (50nM) and harvested at the times shown. (D), as (C) except that HCT116 cells were used. In all cases the extent of protein phosphorylation was determined by Western blotting using the antibodies shown.

Figure S2. ALX does not induce PCNA mono-ubiquitylation. HeLa cells were treated with ALX and harvested at the times shown. Cells were also UV-irradiated ($20J/m^2$) or treated with etoposide (1μM for 8h.). Cells were harvested and the expression of PCNA determined by Western blotting. Multiple exposures of the Western blot are shown.

Figure S3. ALX does not activate the ATM pathway. (A), HeLa cells were treated with ALX (50nM) for the times shown. Western blotting was used to assess the phosphorylation of KAP-1 and Chk2. (B), HeLa cells were treated with ALX (50nM) in the presence and absence of the ATM inhibitor, KU-55933 (10μM). Cells were harvested at the times shown and the extent of protein phosphorylation determined by Western blotting. The efficacy of the ATM inhibitor is shown in the right-hand panel.

Figure S4. ATM is not activated by ALX. (A), HeLa cells were treated with control or ATM inhibitor KU-55933 (10μM) for 24 hours. They were then treated with ALX (50nM) for the times shown, fixed and processed for immunofluorescence microscopy using antibodies against γH2AX and 53BP1. (B), Different γH2AX and 53BP1 staining patterns designated Type I to V in (C). (C), upper panel, γH2AX and 53BP1 staining seen in cells after treatment with the ATM inhibitor but before addition of ALX; lower panel, γH2AX and 53BP1 staining seen in cells treated with ALX for 24 hours.

Figure S5. Claspin expression is required for the full activation of the DNA damage response by ALX. U2OS-shCLSPN cells were treated with doxycycline for 48 hours to reduce Claspin expression. Cells were then treated with ALX (50nM) and harvested at the times shown. The extent of protein phosphorylation was determined by Western blotting.

Figure S6. The DNA-PK but not ATM pathway is activated by ALX in the absence of ATR. (A), DLD1-Seckel cells and DLD1-Seckel cells in the presence of the ATM inhibitor, KU-55933 (10μM) were treated with ALX (50nM) and harvested at the times shown. The extent of protein phosphorylation was determined by Western blotting. Control irradiated cells are shown in the left-hand lanes to verify the activity of the ATM inhibitor. (B), HeLa cells were treated with 50nM ALX in the presence of an ATR inhibitor (5μM) and/or DNA-PK inhibitor (10μM) for the times indicated. The extent of protein phosphorylation was determined by Western blotting.

Figure S7. MSH2, FANCF and RNF8 are not involved in the cellular response to ALX. (A), HeLa cells were treated with control siRNA or siRNA targeted to MSH2. After 72 hours ALX (50nM) was added to the cells, which were then harvested at the times shown. (B), 2008 cells transfected with a control vector or a vector expressing FANCF were treated with ALX (50nM) and then harvested at the times shown. The *FANCF* status of the 2008 cells has been previously verified elsewhere[38]. (C), U2OS cells expressing an inducible RNF8 shRNA were treated with doxycycline for 48 hours and then treated with ALX (50nM). Cells were harvested at the times shown. In all cases protein phosphorylation and expression were determined by Western blotting.

Figure S8. Low dose ALX does not induce autophagy or apoptosis in tumour epithelial cells, although it induces p53 expression. (A), 293 cells stably expressing the GFP-LC3 fusion protein were treated with doses of ALX as shown or serum starved for 4 hours. GFP-LC3 puncta were counted. 293 cells on full medium or serum starved were used as negative and positive controls, respectively. (B), U2OS and (C), H1299 cells were treated with ALX (150nM or 500nM) or cisplatin (10μg/ml) for the times shown. Protein expression was determined by Western blotting. (D), U2OS cells were treated with ALX (50nM) for the times shown. Protein expression was determined by Western blotting.

Figure S9. Oncogene-induced replication stress exacerbates the DDR activated by ALX. (A), hTert-immortalised human fibroblasts were infected with either an empty adenovirus (Ad-Con) or adenovirus expressing Cyclin E (Ad-CycE). The cells were treated with 50nM ALX 48h post-infection for the times indicated and the DDR was monitored by Western blotting. (B), hTert-immortalised BJ skin fibroblasts expressing inducible mutant H-Ras (G12V) were either mock treated or treated with 334nM 4-hydroxy-tamoxifen (4-OHT) for 48h and then exposed to 50nM ALX for the times indicated. Activation of the DDR was monitored by Western blotting using the antibodies indicated. (C), U2OS cells in the presence or absence of tetracycline were exposed

to 3μM ALX for the time indicated and the harvested. Western blot analysis was used to monitor the induction of cell death.

Figure S10. ALX induces apoptosis in T-ALL cell lines. Jurkat, CCRF-CEM and MOLT4 cells were treated with ALX (150nM or 500nM) or cisplatin (10μg/ml) for the times shown. Protein expression was determined by Western blotting as shown.

References

1. Nitiss JL. Targeting DNA topoisomerase II in cancer chemotherapy. *Nat Rev Cancer* 2009; **9**:338-50.

2. Nitiss JL. DNA topoisomerase II and its growing repertoire of biological functions. *Nat Rev Cancer* 2009; 9:327-37.

3. Larsen AK, Escargueil AE, Skladanowski A. Catalytic topoisomerase II inhibitors in cancer therapy. *Pharmacol Ther* 2003; **99**:167-81.

4. Pommier Y. Drugging topoisomerases: lessons and challenges. *ACS Chem Biol* 2013; **8**:82-95.

5. Wang JC. Cellular roles of DNA topoisomerases: a molecular perspective. *Nat Rev Mol Cell Biol* 2002; **3**:430-40.

6. Beeharry N, Rattner JB, Caviston JP, Yen T. Centromere fragmentation is a common mitotic defect of S and G2 checkpoint override. *Cell Cycle* 2013; **12**:1588-97.

7. Al-Ejeh F, Kumar R, Wiegmans A, Lakhani SR, Brown MP, Khanna KK. Harnessing the complexity of DNA-damage response pathways to improve cancer treatment outcomes. *Oncogene* 2010; **29**:6085-98.

8. Longley DB, Johnston PG. Molecular mechanisms of drug resistance. *J Pathol* 2005; **205**:275-92.

9. Pors K, Paniwnyk Z, Teesdale-Spittle P, Plumb JA, Willmore E, Austin CA *et al.* Alchemix: a novel alkylating anthraquinone with potent activity against anthracycline- and cisplatin-resistant ovarian cancer. *Mol Cancer Ther* 2003; **2**:607-10.

10. Pors K, Paniwnyk Z, Ruparelia KC, Teesdale-Spittle PH, Hartley JA, Kelland LR *et al*. Synthesis and biological evaluation of novel chloroethylaminoanthraquinones with potent cytotoxic activity against cisplatin-resistant tumor cells. *J Med Chem* 2004; **47**:1856-9.

11. Abdallah QM, Phillips RM, Johansson F, Helleday T, Cosentino L, Abdel-Rahman H *et al*. Minor structural modifications to alchemix influence mechanism of action and pharmacological activity. *Biochem Pharmacol* 2012; **83**:1514-22.

12. Caldecott K, Banks G, Jeggo P. DNA double-strand break repair pathways and cellular tolerance to inhibitors of topoisomerase II. *Cancer Res* 1990; **50**:5778-83.

13. Forrest RA, Swift LP, Evison BJ, Rephaeli A, Nudelman A, Phillips DR *et al*. The hydroxyl epimer of doxorubicin controls the rate of formation of cytotoxic anthracycline-DNA adducts. *Cancer Chemother Pharmacol* 2013; **71**:809-16.

14. Ward IM, Chen J. Histone H2AX is phosphorylated in an ATR-dependent manner in response to replicational stress. *J Biol Chem* 2001; **276**:47759-62.

15. Yajima H, Lee KJ, Chen BP. ATR-dependent phosphorylation of DNA-dependent protein kinase catalytic subunit in response to UV-induced replication stress. *Mol Cell Biol* 2006; **26**:7520-8.

16. Yajima H, Lee KJ, Zhang S, Kobayashi J, Chen BP. DNA double-strand break formation upon UV-induced replication stress activates ATM and DNA-PKcs kinases. *J Mol Biol* 2009; **385**:800-10.

17. McNeely S, Conti C, Sheikh T, Patel H, Zabludoff S, Pommier Y *et al*. Chk1 inhibition after replicative stress activates a double strand break response mediated by ATM and DNA-dependent protein kinase. *Cell Cycle* 2010; **9**:995-1004.

18. Wang Y, Qin J. MSH2 and ATR form a signaling module and regulate two branches of the damage response to DNA methylation. *Proc Natl Acad Sci USA* 2003; **100**:15387-92.

19. Pabla N, Ma Z, McIlhatton MA, Fishel R, Dong Z. hMSH2 recruits ATR to DNA damage sites for activation during DNA damage-induced apoptosis. *J Biol Chem* 2011; **286**:10411-8.

20. Pors K, Patterson LH. DNA mismatch repair deficiency, resistance to cancer chemotherapy and the development of hypersensitive agents. *Curr Top Med Chem* 2005; **5**:1133-49.

21. Pors K, Plumb JA, Brown R, Teesdale-Spittle P, Searcey M, Smith PJ *et al*. Development of nonsymmetrical 1, 4-disubstituted anthraquinones that are potently active against cisplatin-resistant ovarian cancer cells. *J Med Chem* 2005; **48**:6690-5

22. Sy SM, Jiang J, Dong SS, Lok GT, Wu J, Cai H et al. Critical roles of ring finger protein RNF8 in replication stress responses. *J Biol Chem* 2011; **286**:22355-61.

23. Orth JD, Loewer A, Lahav G, Mitchison TJ. Prolonged mitotic arrest triggers partial activation of apoptosis, resulting in DNA damage and p53 induction. *Mol Biol Cell* 2012; **23**:567-76.

24. Bester AC, Roniger M, Oren YS, Im MM, Sarni D, Chaoat M, *et al*. Nucleotide deficiency promotes genomic instability in early stages of cancer development. *Cell* 2011; **145**:435-46.

25. Jones RM, Mortusewicz O, Afzal I, Lorvellec M, García P, Helleday T *et al*. Increased replication initiation and conflicts with transcription underlie Cyclin E-induced replication stress. *Oncogene* 2013; **32**:3744-53.

26. Stankovic T, Weber P, Stewart G, Bedenham T, Murray J, Byrd PJ *et al.* Inactivation of ataxia telangiectasia mutated gene in B-cell chronic lymphocytic leukaemia. *Lancet* 1999; **353**:26-9

27. Vorechovský I, Luo L, Dyer MJ, Catovsky D, Amlot PL, Yaxley JC *et al.* Clustering of missense mutations in the ataxia-telangiectasia gene in a sporadic T-cell leukaemia. *Nat Genet* 1997; **17**:96-9.

28. Schaffner C, Idler I, Stilgenbauer S, Döhner H, Lichter P. Mantle cell lymphoma is characterized by inactivation of the ATM gene. *Proc Natl Acad Sci USA* 2000; **97**:2773-8

29. Bhojwani D, Pui CH. Relapsed childhood acute lymphoblastic leukaemia. *Lancet Oncol.* 2013;**14**:e205-17.

30. Inaba H, Greaves M, Mullighan CG. Acute lymphoblastic leukaemia. *Lancet* 2013**; 81**:1943-55.

31. Hof J, Krentz S, van Schewick C, Körner G, Shalapour S, Rhein P *et al*. Mutations and deletions of the TP53 gene predict nonresponse to treatment and poor outcome in first relapse of childhood acute lymphoblastic leukemia. *J Clin Oncol* 2011; **29**:3185-93.

32. Holmfeldt L, Wei L, Diaz-Flores E, Walsh M, Zhang J, Ding L *et al*. The genomic landscape of hypodiploid acute lymphoblastic leukemia. *Nat Genet* 2013; **45**:242-52.

33. Chan EY, Kir S, Tooze SA. siRNA screening of the kinome identifies ULK1 as a multidomain modulator of autophagy. *J Biol Chem* 2007; **282**:25464-74.

34. Greaves M. (2013) Return of the malingering mutants. *Br J Cancer* 2013; **109**:1391-3.

35. Redmond KM, Wilson TR, Johnston PG, Longley DB. Resistance mechanisms to cancer chemotherapy. *Front Biosci* 2008; **13**:5138-54.

36. Stewart GS, Panier S, Townsend K, Al-Hakim AK, Kolas NK, Miller ES *et al*. The RIDDLE syndrome protein mediates a ubiquitin-dependent signaling cascade at sites of DNA damage. *Cell* 2009; **136**:420-34.

37. Petermann E, Orta ML, Issaeva N, Schultz N, Helleday T. Hydroxyurea-stalled replication forks become progressively inactivated and require two different RAD51-mediated pathways for restart and repair. *Mol Cell* 2010; **37**:492-502.

38. Taniguchi T, Tischkowitz M, Ameziane N, Hodgson SV, Mathew CG, Joenje H *et al.* Disruption of the Fanconi anemia-BRCA pathway in cisplatin-sensitive ovarian tumors. *Nat Med* 2003; **9**:568-74.

Fig. 1

A

U2OS

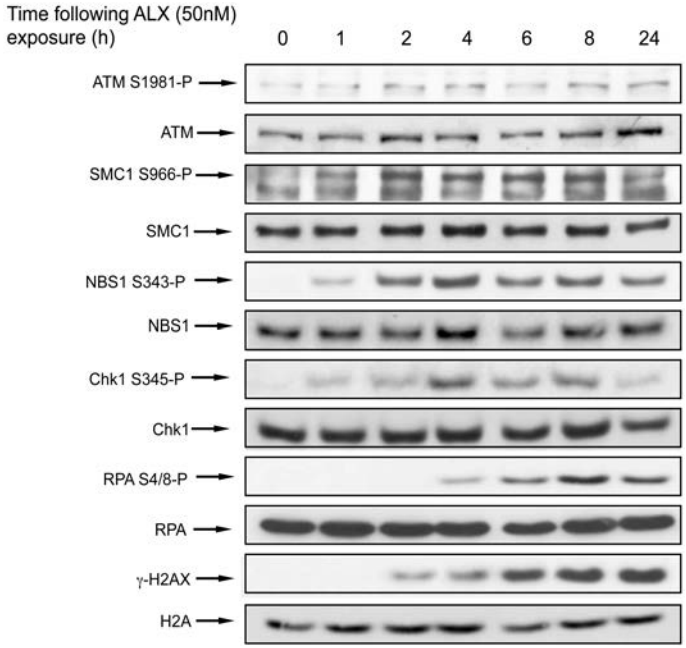

B

H1299

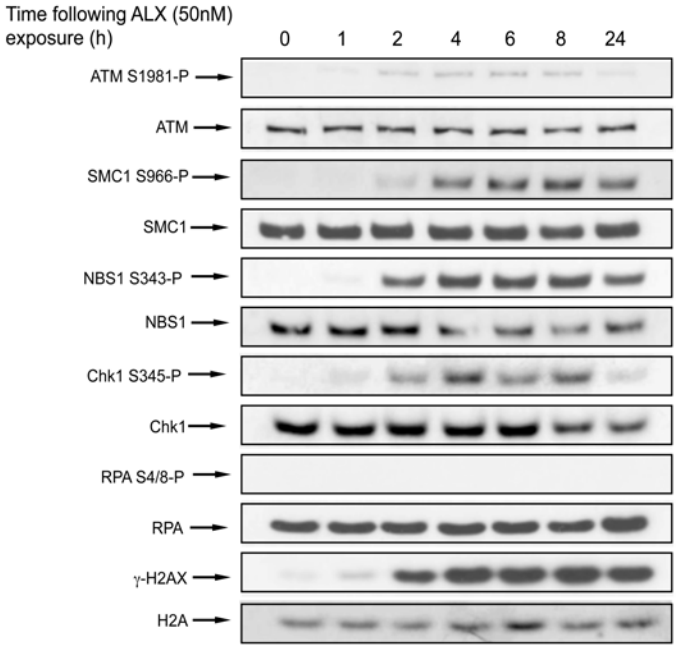

C

HeLa

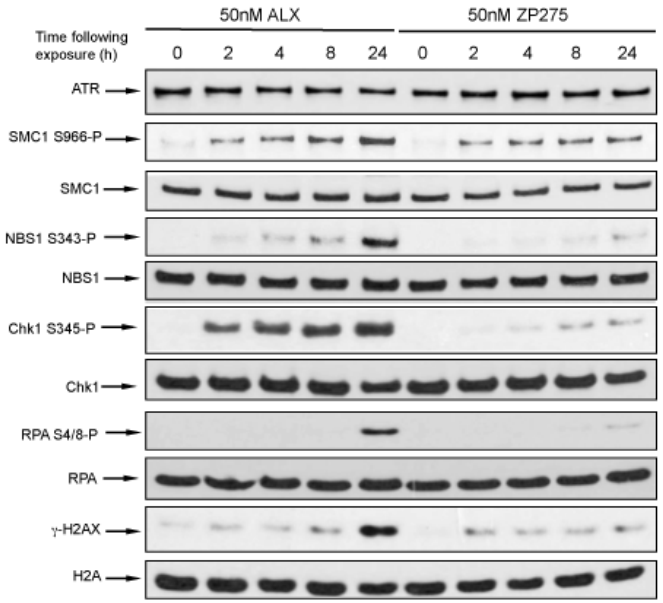

Fig. 2

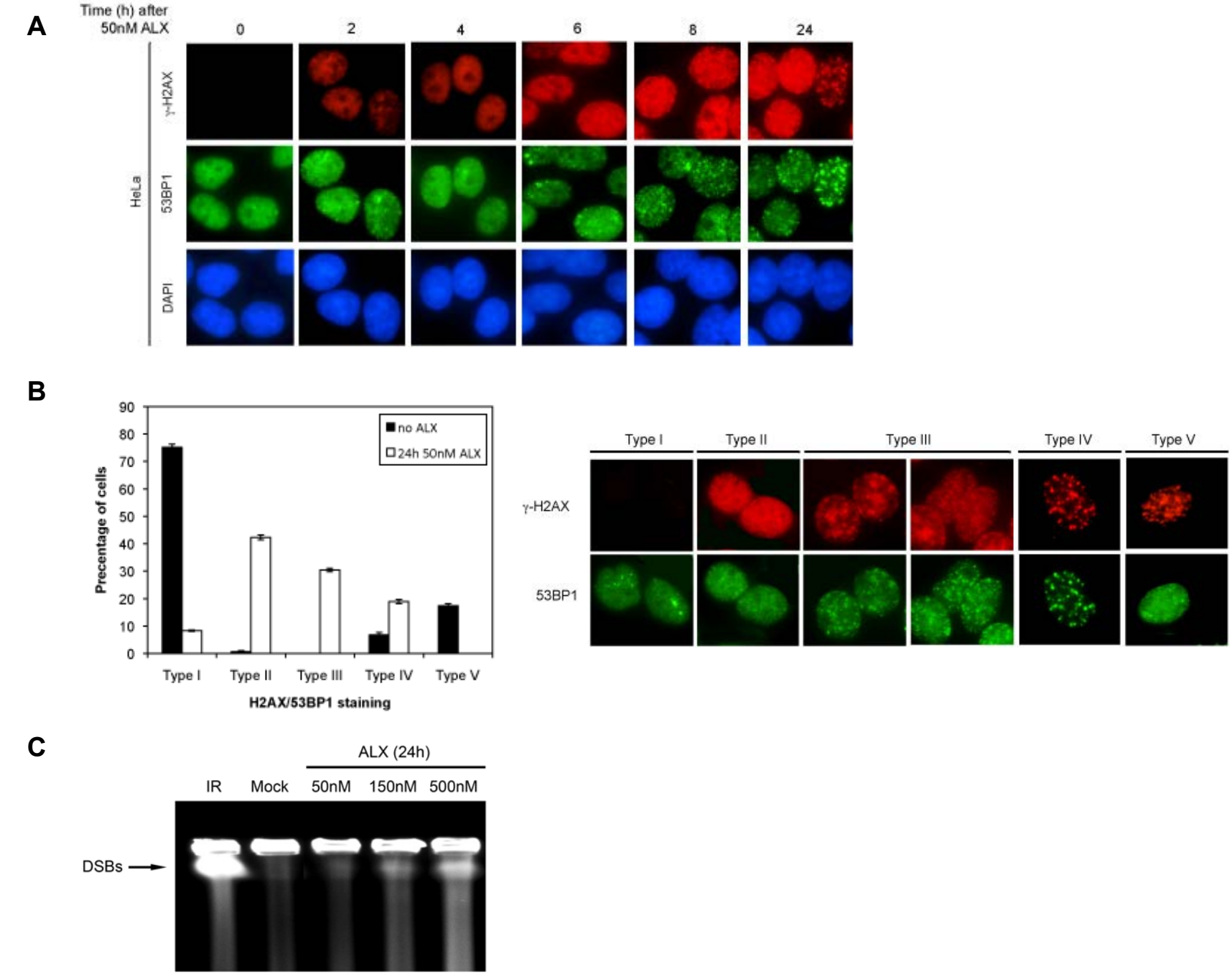
A
Time (h) after 50nM ALX
0
2
4
6
8
24
HeLa
γ-H2AX
53BP1
DAPI
B
Precentage of cells
no ALX
24h 50nM ALX
Type I
Type II
Type III
Type IV
Type V
H2AX/53BP1 staining
γ-H2AX
53BP1
C
ALX (24h)
IR
Mock
50nM
150nM
500nM
DSBs

Fig. 3

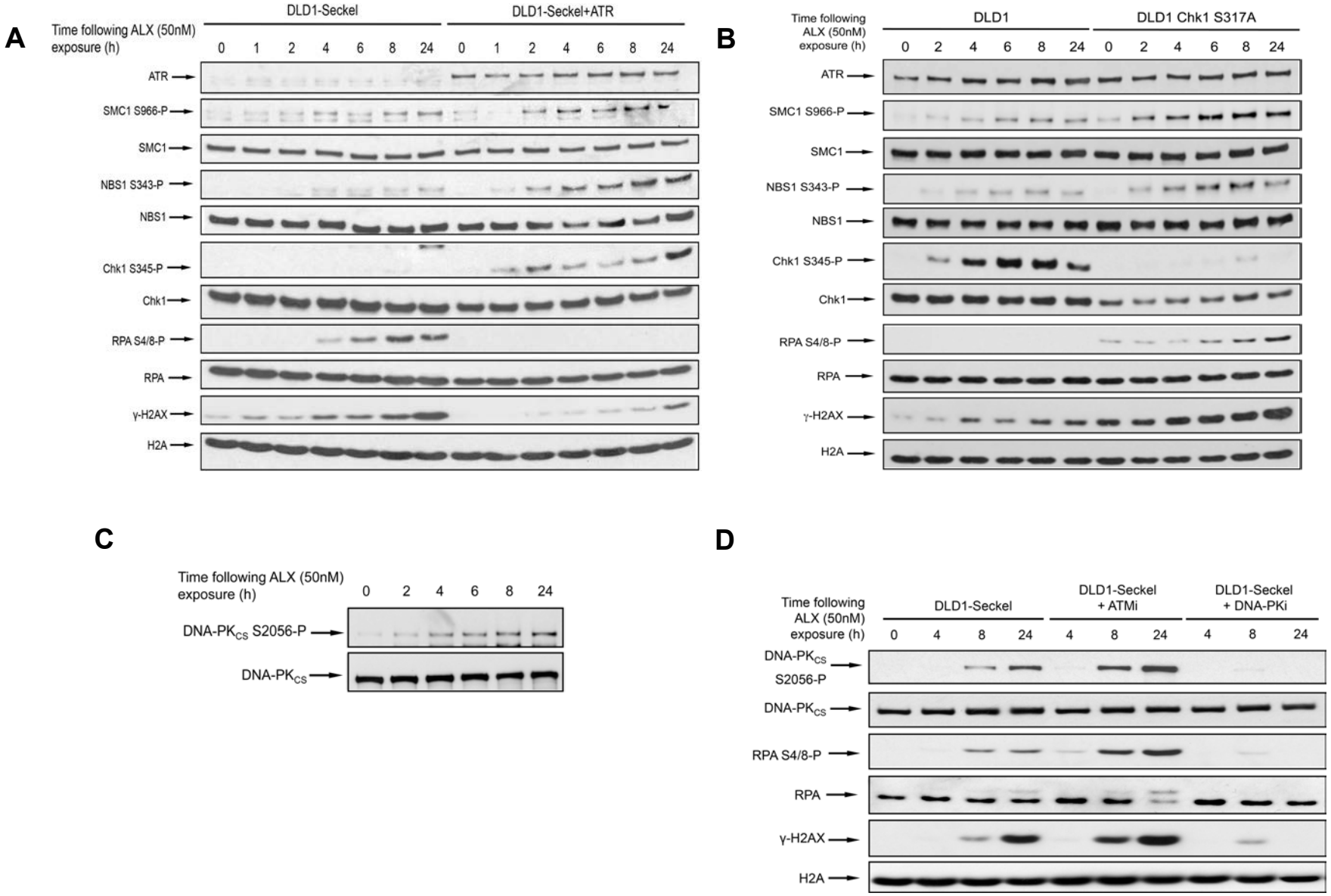
A
Time following ALX (50nM) exposure (h)
DLD1-Seckel
DLD1-Seckel+ATR
0 1 2 4 6 8 24 0 1 2 4 6 8 24
ATR
SMC1 S966-P
SMC1
NBS1 S343-P
NBS1
Chk1 S345-P
Chk1
RPA S4/8-P
RPA
γ-H2AX
H2A
B
Time following ALX (50nM) exposure (h)
DLD1
DLD1 Chk1 S317A
0 2 4 6 8 24 0 2 4 6 8 24
ATR
SMC1 S966-P
SMC1
NBS1 S343-P
NBS1
Chk1 S345-P
Chk1
RPA S4/8-P
RPA
γ-H2AX
H2A
C
Time following ALX (50nM) exposure (h)
0 2 4 6 8 24
DNA-PKcs S2056-P
DNA-PKcs
D
Time following ALX (50nM) exposure (h)
DLD1-Seckel
DLD1-Seckel + ATMi
DLD1-Seckel + DNA-PKi
0 4 8 24 4 8 24 4 8 24
DNA-PKcs S2056-P
DNA-PKcs
RPA S4/8-P
RPA
γ-H2AX
H2A

Fig. 4

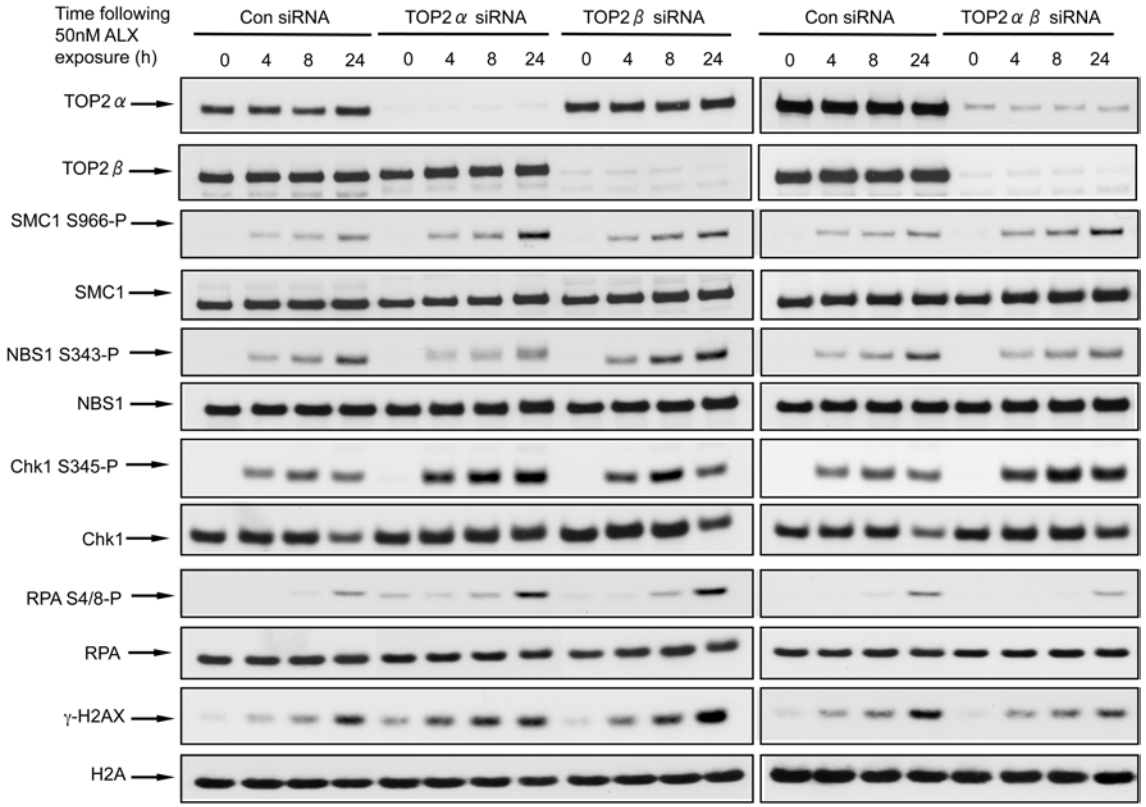
Time following 50nM ALX exposure (h)
Con siRNA
TOP2α siRNA
TOP2β siRNA
Con siRNA
TOP2α β siRNA
0 4 8 24 0 4 8 24 0 4 8 24 0 4 8 24 0 4 8 24
TOP2α
TOP2β
SMC1 S966-P
SMC1
NBS1 S343-P
NBS1
Chk1 S345-P
Chk1
RPA S4/8-P
RPA
γ-H2AX
H2A

Fig. 5

A

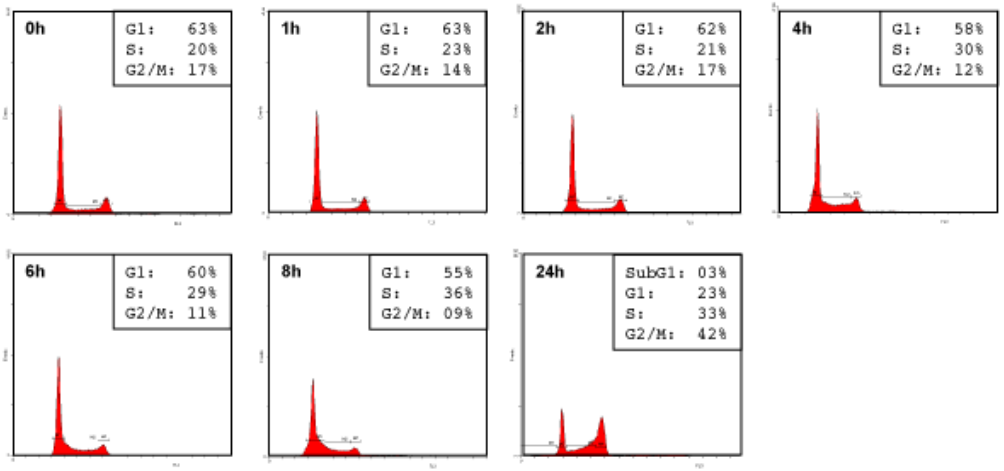
0h
G1: 63%
S: 20%
G2/M: 17%
1h
G1: 63%
S: 23%
G2/M: 14%
2h
G1: 62%
S: 21%
G2/M: 17%
4h
G1: 58%
S: 30%
G2/M: 12%
6h
G1: 60%
S: 29%
G2/M: 11%
8h
G1: 55%
S: 36%
G2/M: 09%
24h
SubG1: 03%
G1: 23%
S: 33%
G2/M: 42%

B

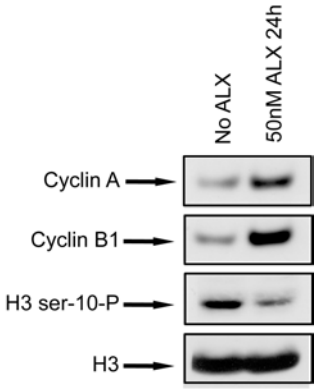
No ALX
50nM ALX 24h
Cyclin A
Cyclin B1
H3 ser-10-P
H3

C

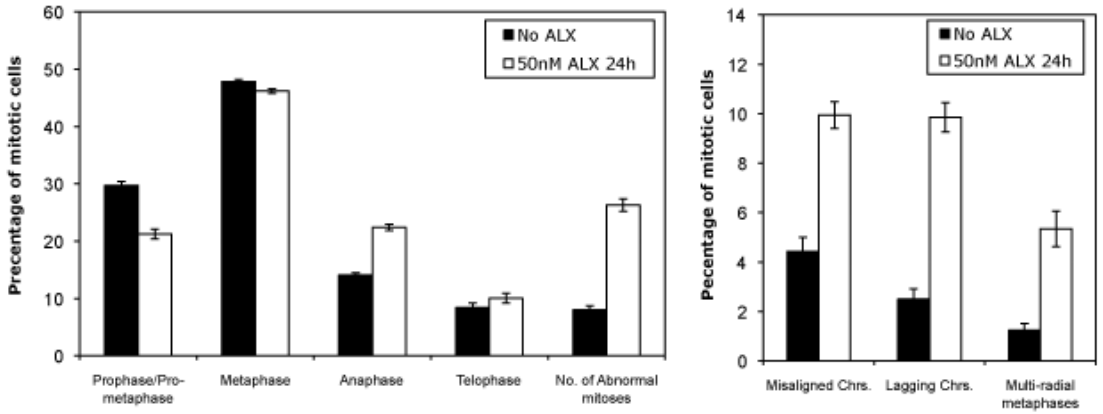
Precentage of mitotic cells
No ALX
50nM ALX 24h
Prophase/Pro-metaphase
Metaphase
Anaphase
Telophase
No. of Abnormal mitoses
Pecentage of mitotic cells
Misaligned Chrs.
Lagging Chrs.
Multi-radial metaphases

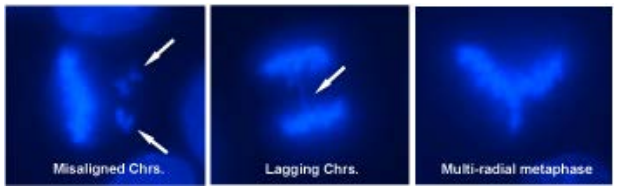
Misaligned Chrs.
Lagging Chrs.
Multi-radial metaphase

Fig. 6

A

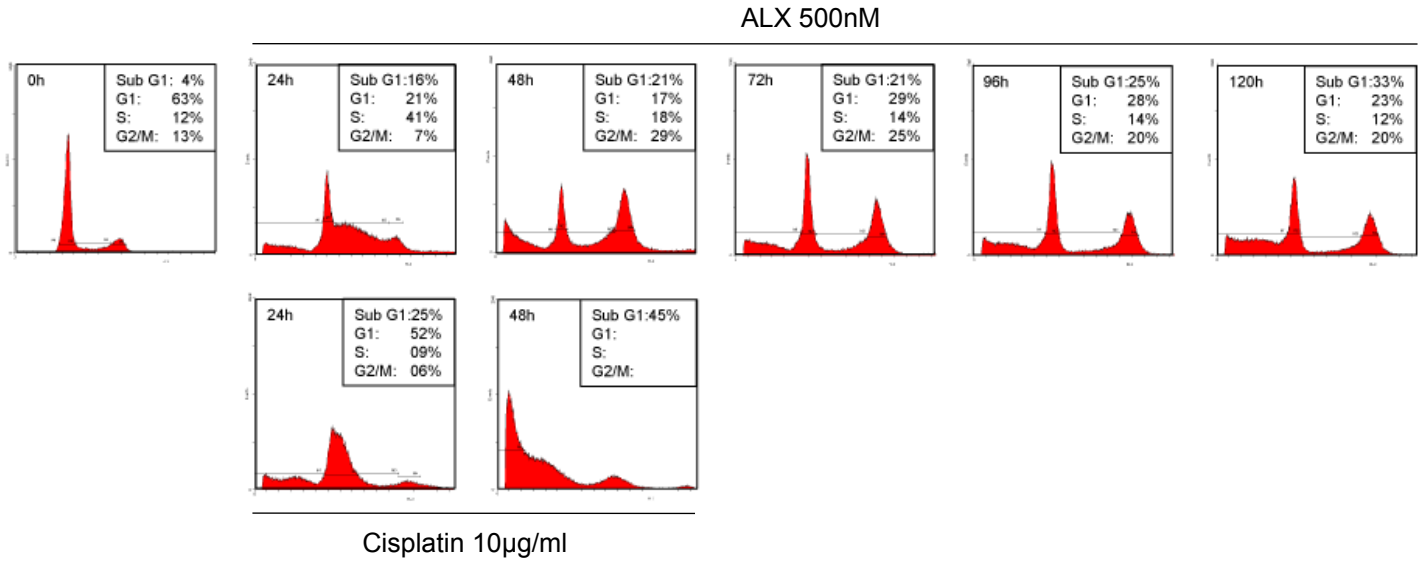
ALX 500nM
0h
Sub G1: 4%
G1: 63%
S: 12%
G2/M: 13%
24h
Sub G1:16%
G1: 21%
S: 41%
G2/M: 7%
48h
Sub G1:21%
G1: 17%
S: 18%
G2/M: 29%
72h
Sub G1:21%
G1: 29%
S: 14%
G2/M: 25%
96h
Sub G1:25%
G1: 28%
S: 14%
G2/M: 20%
120h
Sub G1:33%
G1: 23%
S: 12%
G2/M: 20%
24h
Sub G1:25%
G1: 52%
S: 09%
G2/M: 06%
48h
Sub G1:45%
G1:
S:
G2/M:
Cisplatin 10μg/ml

B

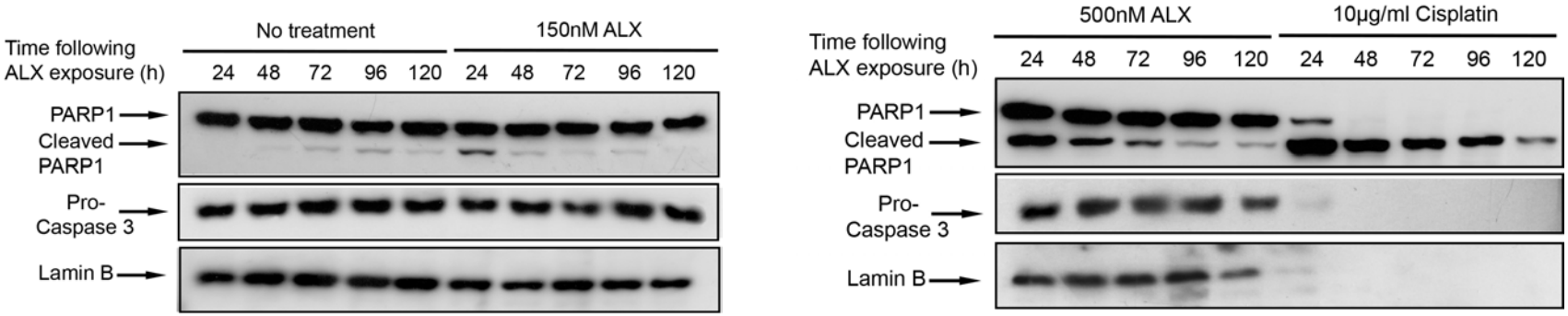
Time following ALX exposure (h)
No treatment
150nM ALX
24 48 72 96 120 24 48 72 96 120
PARP1
Cleaved PARP1
Pro-Caspase 3
Lamin B
Time following ALX exposure (h)
500nM ALX
10μg/ml Cisplatin
24 48 72 96 120 24 48 72 96 120
PARP1
Cleaved PARP1
Pro-Caspase 3
Lamin B

Fig. 6

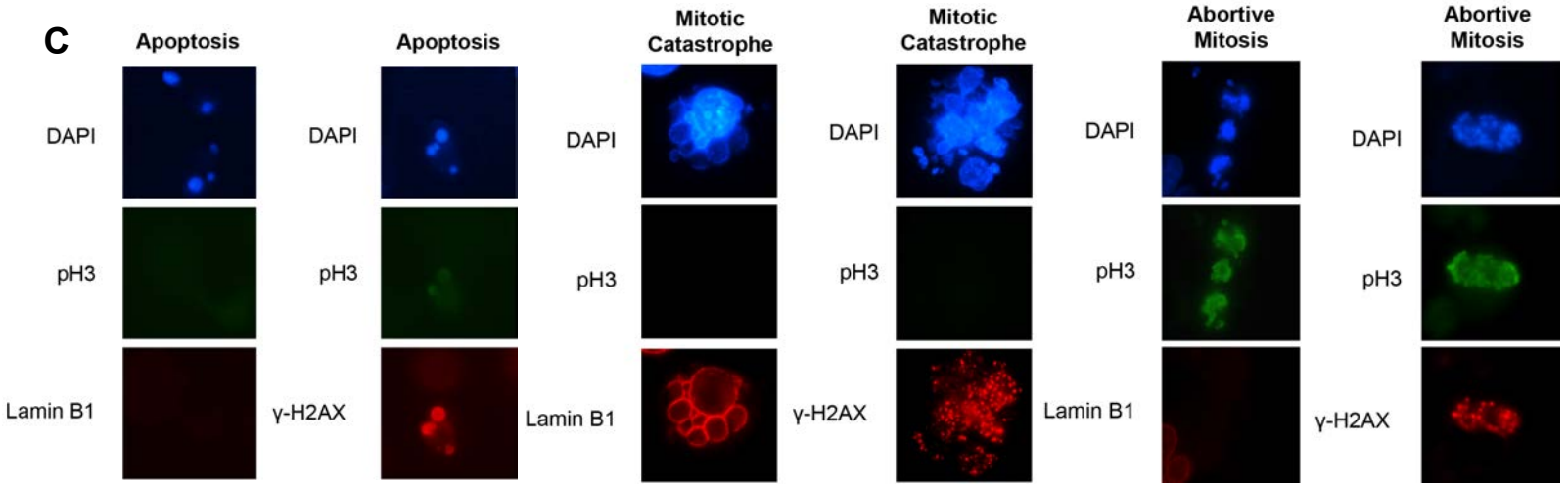
C
Apoptosis
Apoptosis
Mitotic Catastrophe
Mitotic Catastrophe
Abortive Mitosis
Abortive Mitosis
DAPI
pH3
Lamin B1
γ-H2AX

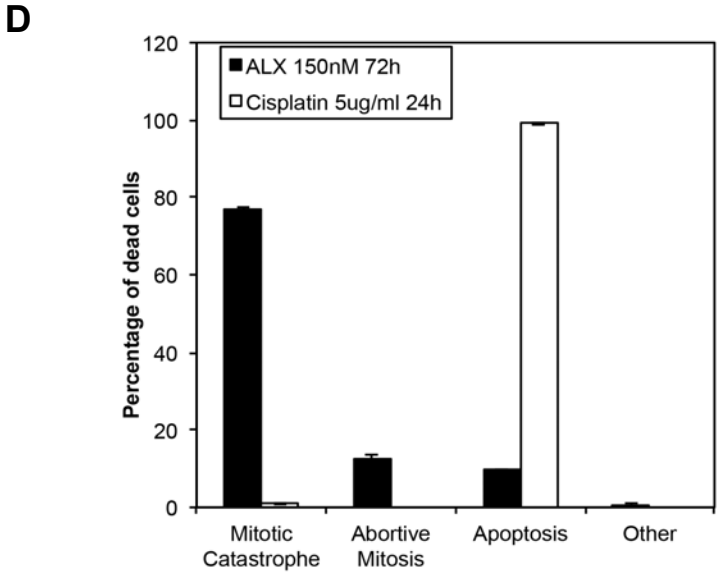
D
ALX 150nM 72h
Cisplatin 5ug/ml 24h
Percentage of dead cells
120
100
80
60
40
20
0
Mitotic Catastrophe
Abortive Mitosis
Apoptosis
Other

Fig. 7

A

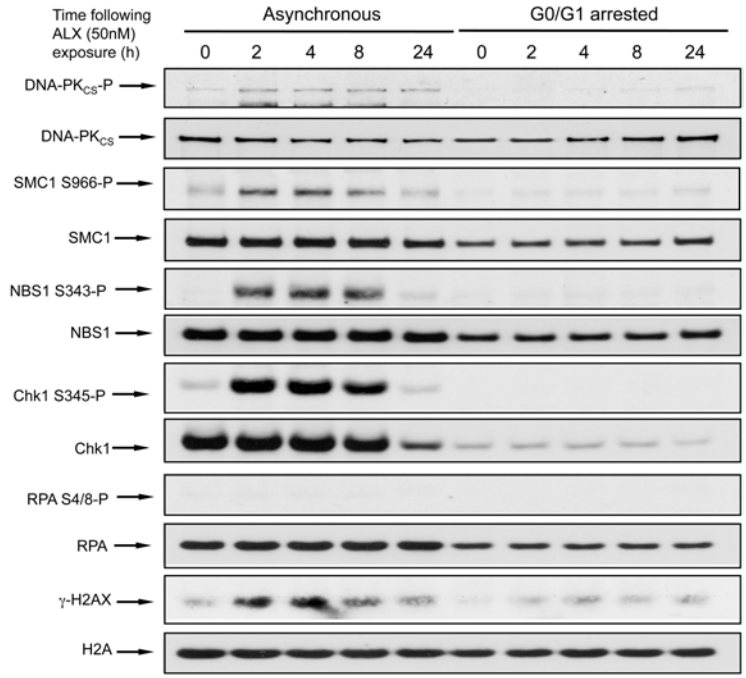
Time following ALX (50nM) exposure (h)
Asynchronous
G0/G1 arrested
0 2 4 8 24 0 2 4 8 24
DNA-PKcs-P
DNA-PKcs
SMC1 S966-P
SMC1
NBS1 S343-P
NBS1
Chk1 S345-P
Chk1
RPA S4/8-P
RPA
γ-H2AX
H2A

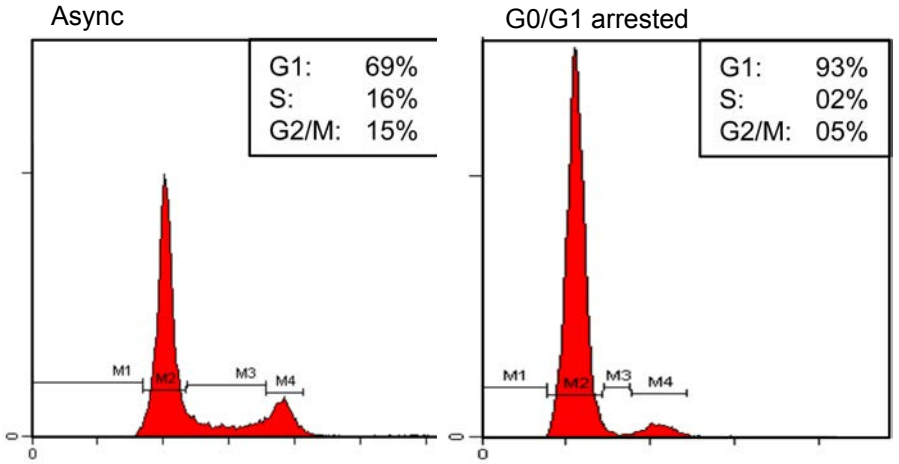
Async
G1: 69%
S: 16%
G2/M: 15%
M1
M2
M3
M4
G0/G1 arrested
G1: 93%
S: 02%
G2/M: 05%
M1
M2
M3
M4

B

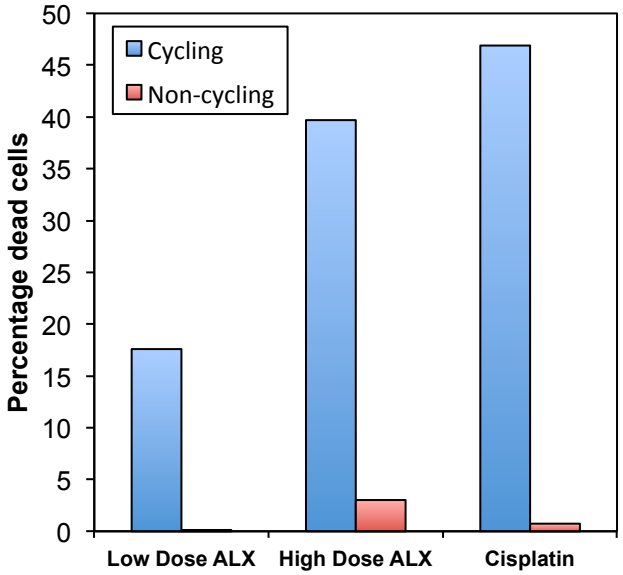
Percentage dead cells
50
45
40
35
30
25
20
15
10
5
0
Cycling
Non-cycling
Low Dose ALX
High Dose ALX
Cisplatin

Fig. 7

C

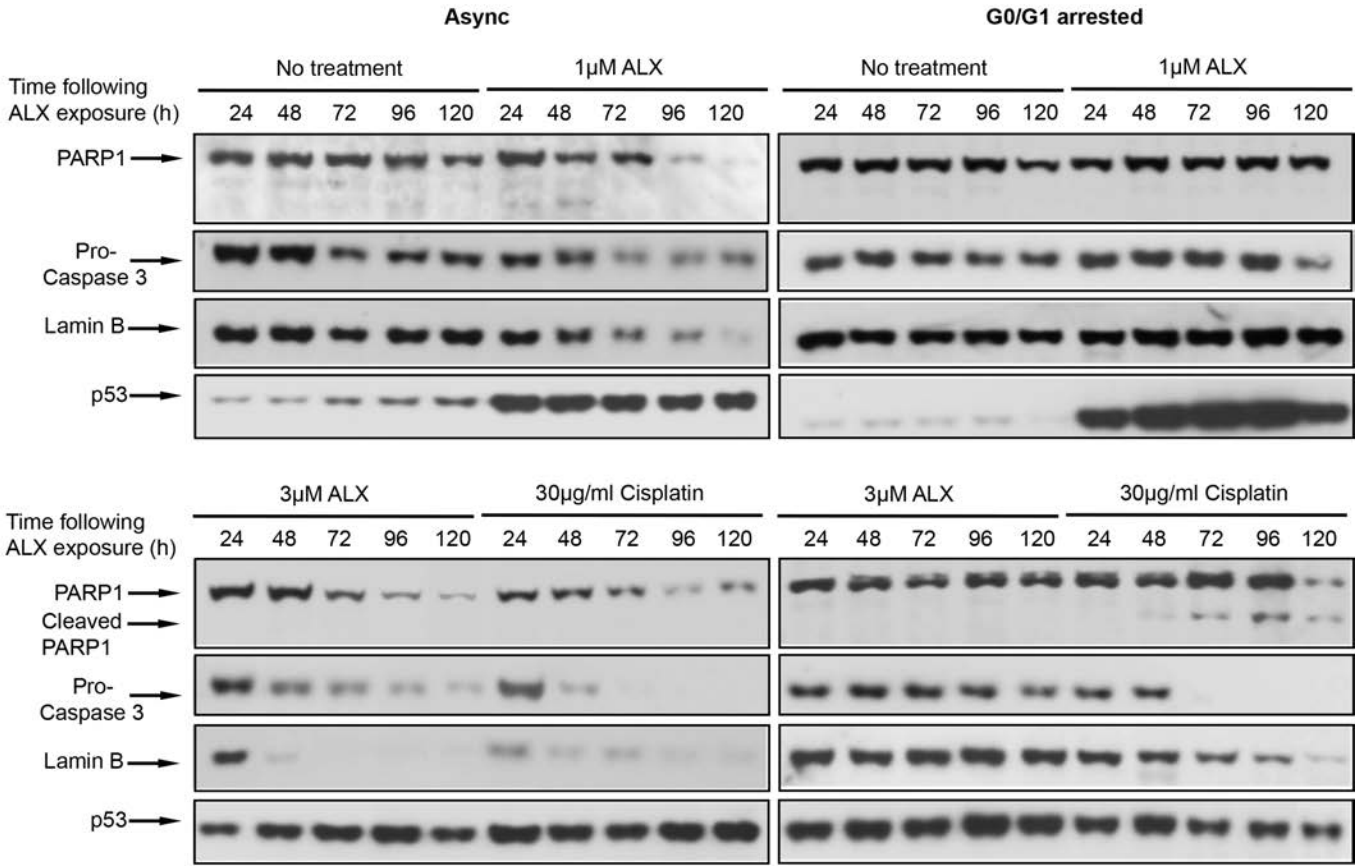
Async
G0/G1 arrested
No treatment
1μM ALX
No treatment
1μM ALX
Time following ALX exposure (h)
24 48 72 96 120 24 48 72 96 120
24 48 72 96 120 24 48 72 96 120
PARP1
Pro-Caspase 3
Lamin B
p53
3μM ALX
30μg/ml Cisplatin
3μM ALX
30μg/ml Cisplatin
Time following ALX exposure (h)
24 48 72 96 120 24 48 72 96 120
24 48 72 96 120 24 48 72 96 120
PARP1
Cleaved PARP1
Pro-Caspase 3
Lamin B
p53

Fig. 8

A

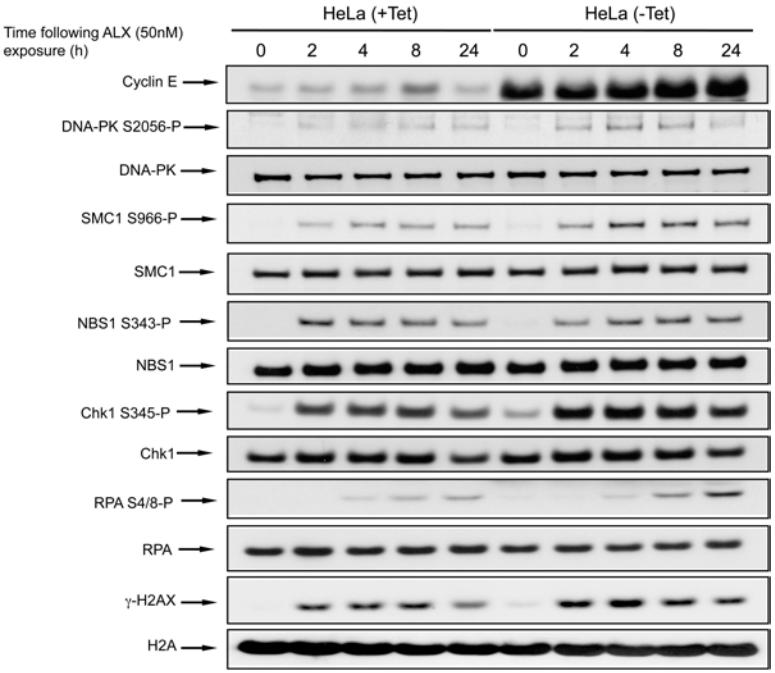
Time following ALX (50nM) exposure (h)
HeLa (+Tet)
HeLa (-Tet)
0 2 4 8 24 0 2 4 8 24
Cyclin E
DNA-PK S2056-P
DNA-PK
SMC1 S966-P
SMC1
NBS1 S343-P
NBS1
Chk1 S345-P
Chk1
RPA S4/8-P
RPA
γ-H2AX
H2A

B

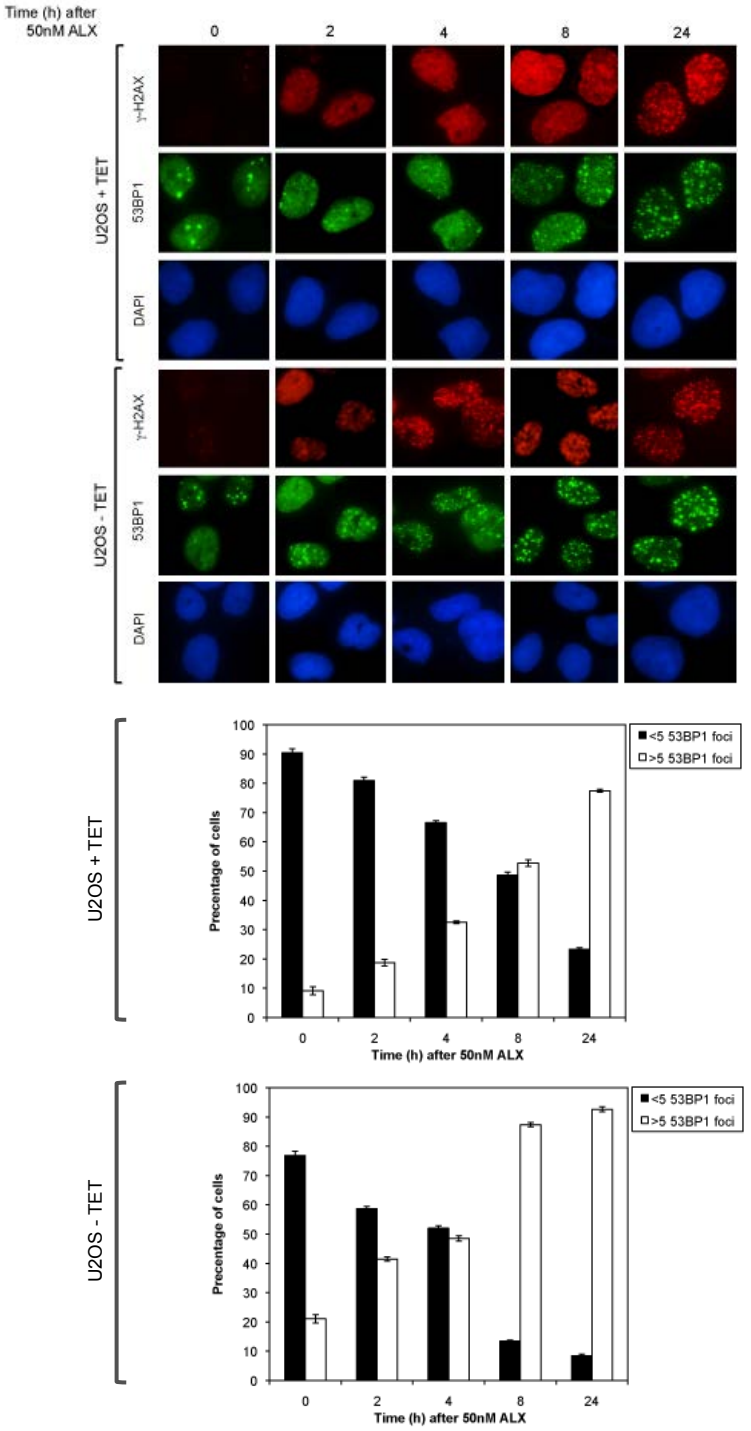
Time (h) after 50nM ALX
0 2 4 8 24
U2OS + TET
γ-H2AX
53BP1
DAPI
U2OS - TET
γ-H2AX
53BP1
DAPI
U2OS + TET
Precentage of cells
<5 53BP1 foci
>5 53BP1 foci
Time (h) after 50nM ALX
U2OS - TET
Precentage of cells
<5 53BP1 foci
>5 53BP1 foci
Time (h) after 50nM ALX

Fig. 9

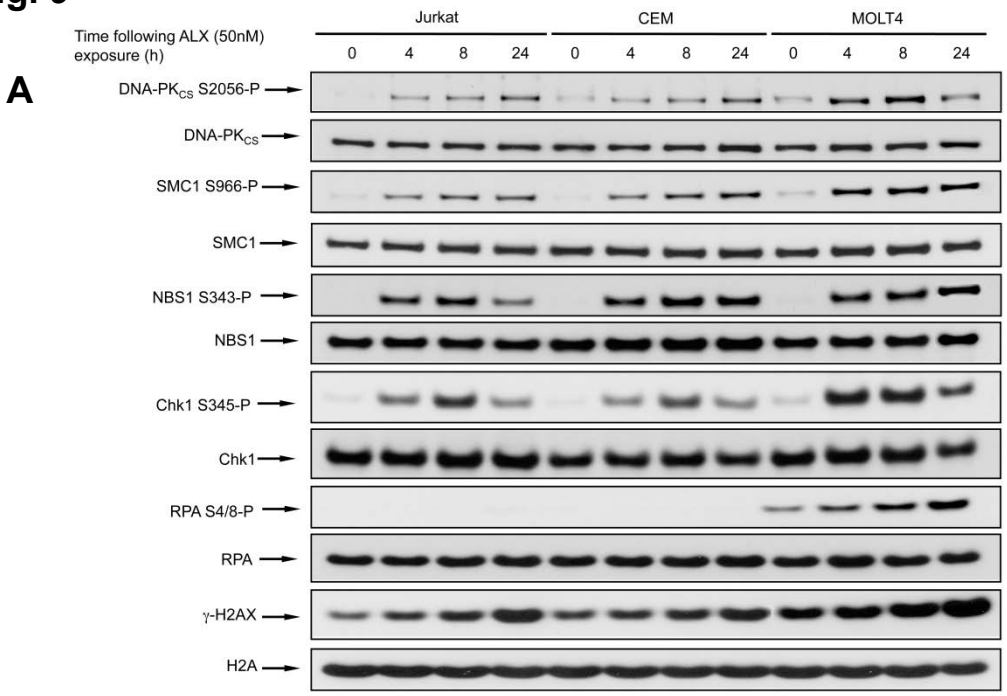
A
Time following ALX (50nM) exposure (h)
Jurkat
CEM
MOLT4
0 4 8 24 0 4 8 24 0 4 8 24
DNA-PKcs S2056-P
DNA-PKcs
SMC1 S966-P
SMC1
NBS1 S343-P
NBS1
Chk1 S345-P
Chk1
RPA S4/8-P
RPA
γ-H2AX
H2A

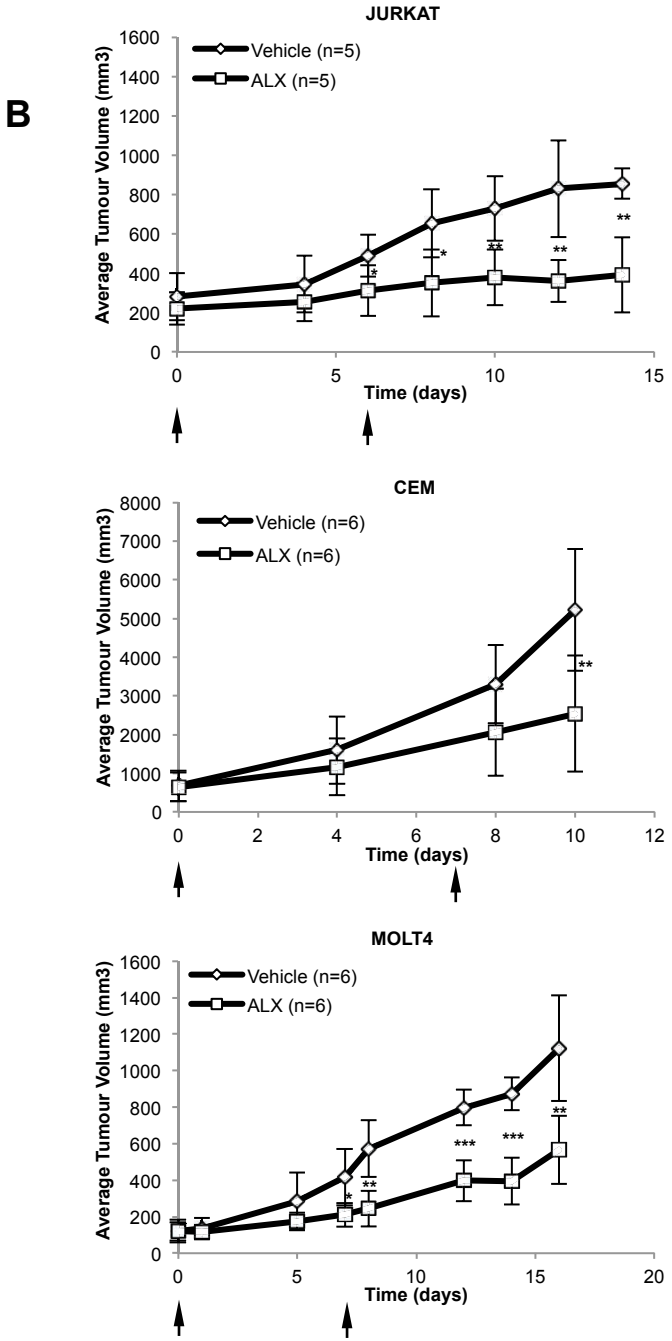
B
JURKAT
Vehicle (n=5)
ALX (n=5)
Average Tumour Volume (mm3)
Time (days)
CEM
Vehicle (n=6)
ALX (n=6)
Average Tumour Volume (mm3)
Time (days)
MOLT4
Vehicle (n=6)
ALX (n=6)
Average Tumour Volume (mm3)
Time (days)

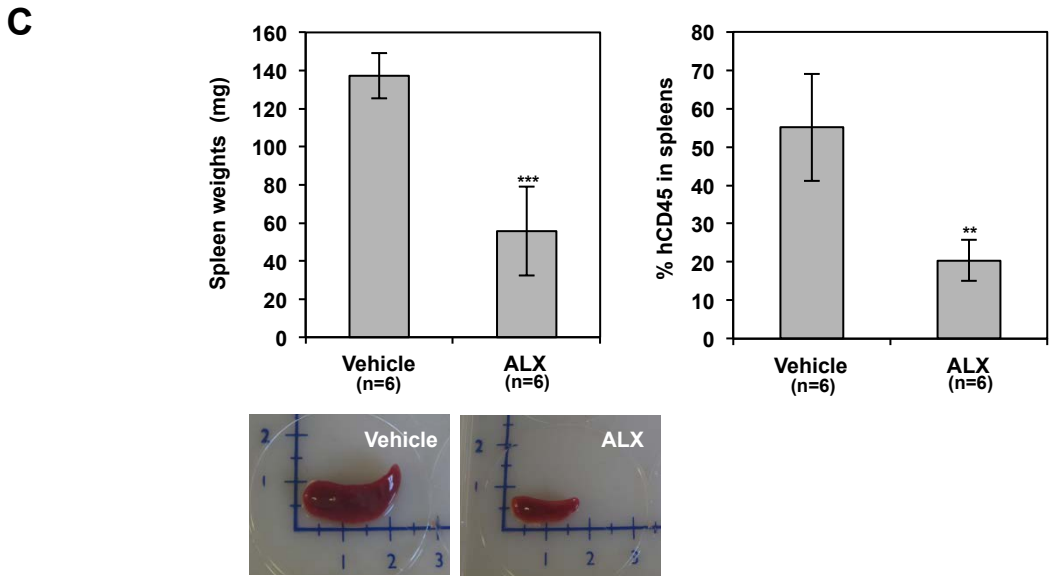
C
Spleen weights (mg)
Vehicle (n=6)
ALX (n=6)
% hCD45 in spleens
Vehicle (n=6)
ALX (n=6)
Vehicle
ALX

Fig. 10

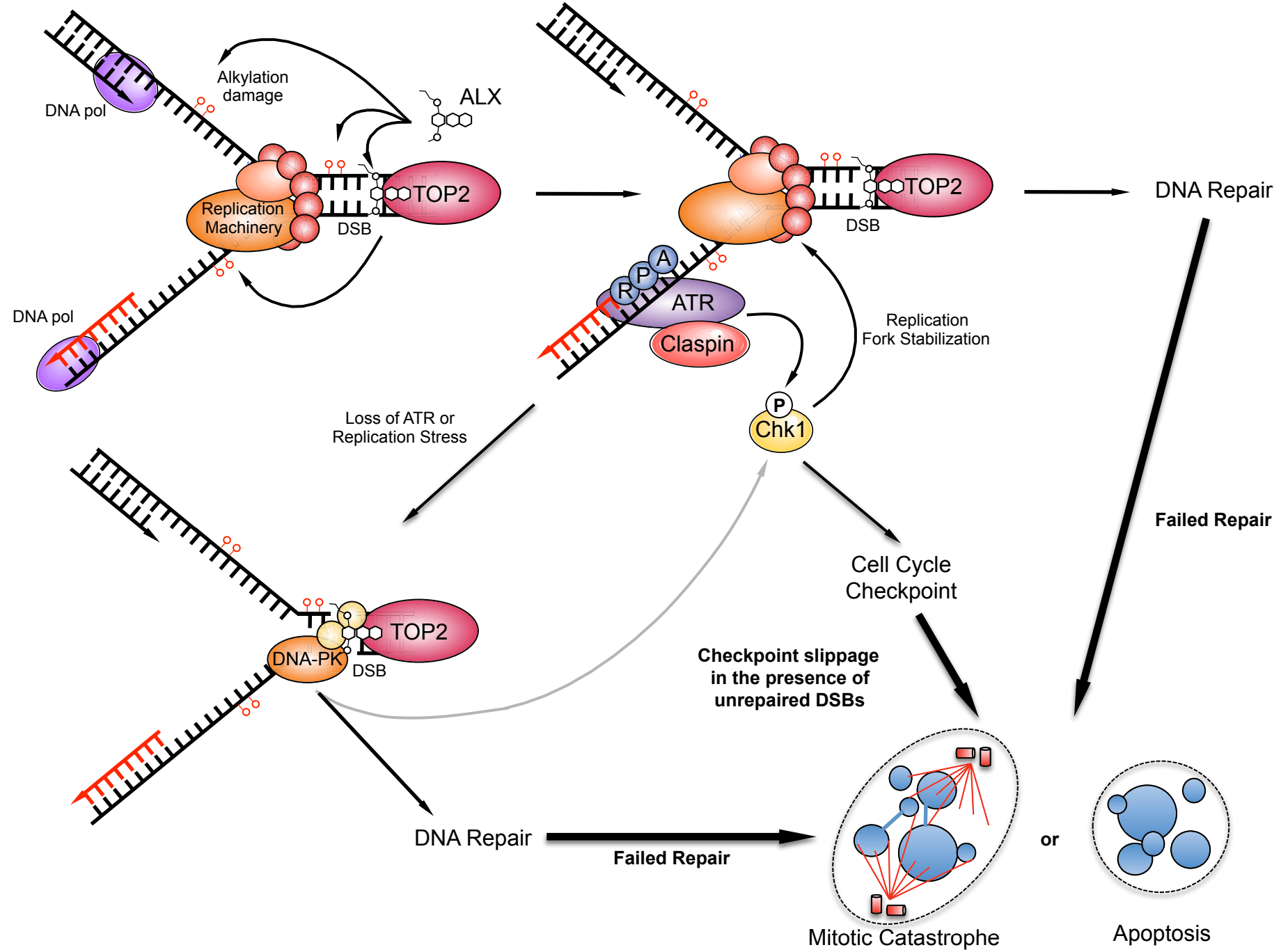
DNA pol
Alkylation damage
ALX
TOP2
Replication Machinery
DSB
DNA pol
TOP2
DSB
DNA Repair
A
P
R
ATR
Claspin
Replication Fork Stabilization
Loss of ATR or Replication Stress
P
Chk1
Failed Repair
Cell Cycle Checkpoint
TOP2
DNA-PK
DSB
Checkpoint slippage in the presence of unrepaired DSBs
DNA Repair
Failed Repair
or
Mitotic Catastrophe
Apoptosis

Fig. S1

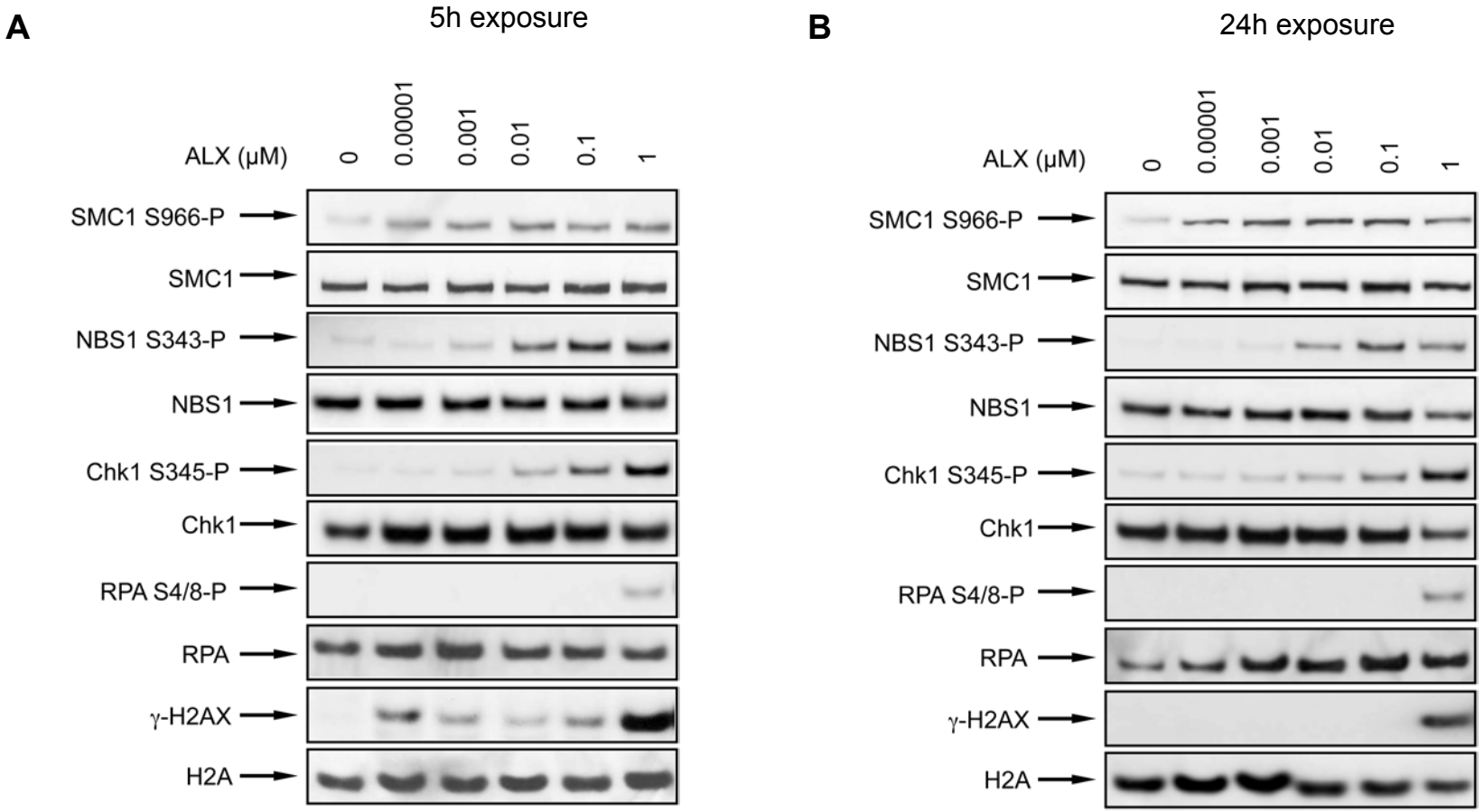
A
5h exposure
ALX (μM)
0
0.00001
0.001
0.01
0.1
1
SMC1 S966-P
SMC1
NBS1 S343-P
NBS1
Chk1 S345-P
Chk1
RPA S4/8-P
RPA
γ-H2AX
H2A
B
24h exposure
ALX (μM)
0
0.00001
0.001
0.01
0.1
1
SMC1 S966-P
SMC1
NBS1 S343-P
NBS1
Chk1 S345-P
Chk1
RPA S4/8-P
RPA
γ-H2AX
H2A

Fig. S1

C

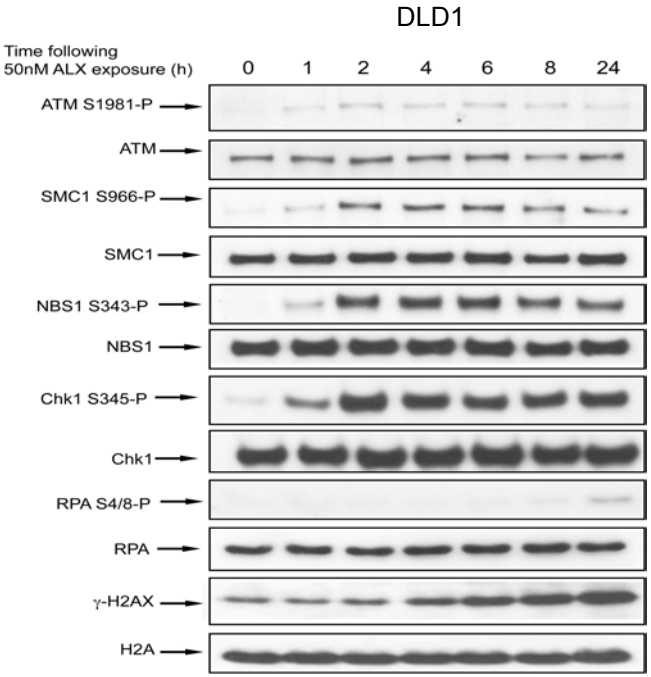
DLD1
Time following
50nM ALX exposure (h)
0 1 2 4 6 8 24
ATM S1981-P
ATM
SMC1 S966-P
SMC1
NBS1 S343-P
NBS1
Chk1 S345-P
Chk1
RPA S4/8-P
RPA
γ-H2AX
H2A

D

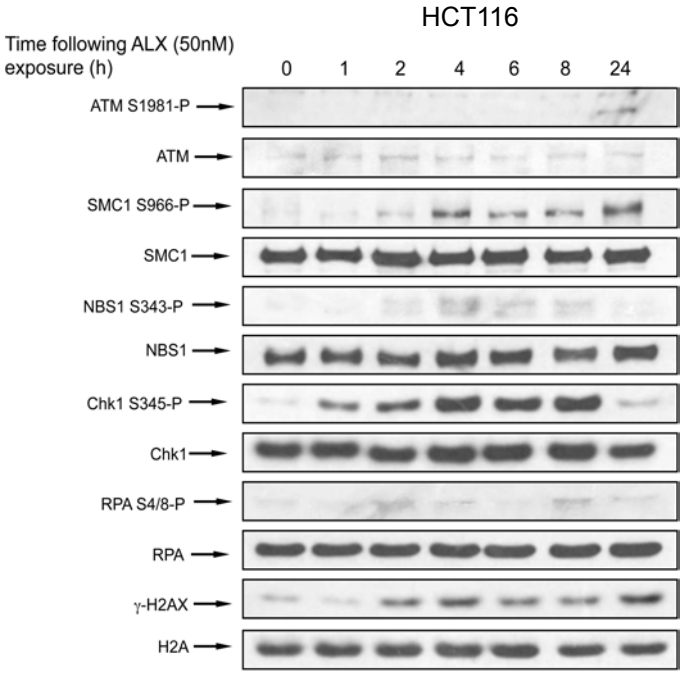
HCT116
Time following ALX (50nM)
exposure (h)
0 1 2 4 6 8 24
ATM S1981-P
ATM
SMC1 S966-P
SMC1
NBS1 S343-P
NBS1
Chk1 S345-P
Chk1
RPA S4/8-P
RPA
γ-H2AX
H2A

Fig. S2

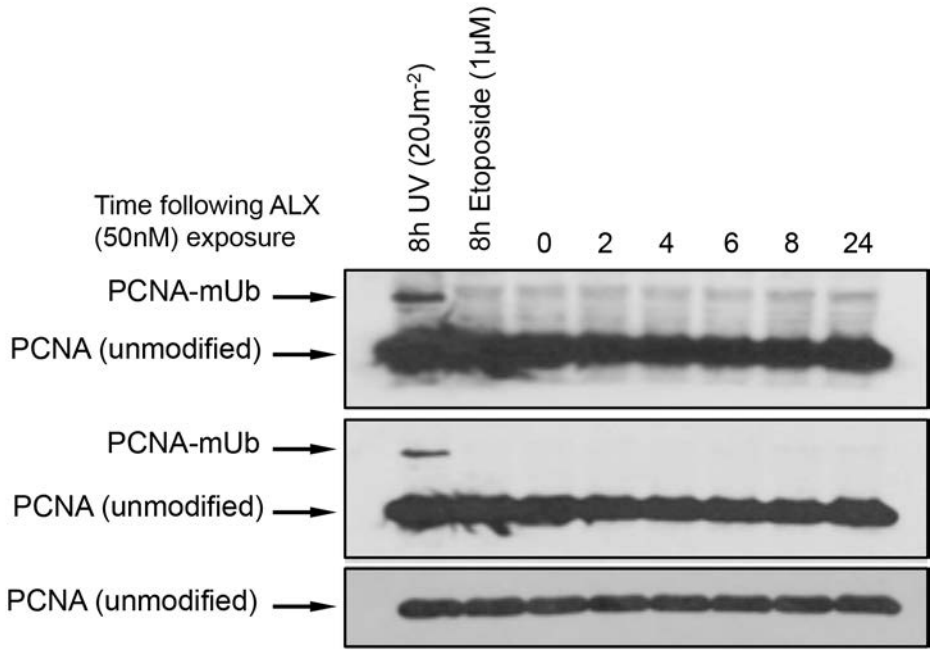
Time following ALX
(50nM) exposure
8h UV (20Jm-2)
8h Etoposide (1μM)
0
2
4
6
8
24
PCNA-mUb
PCNA (unmodified)
PCNA-mUb
PCNA (unmodified)
PCNA (unmodified)

Fig. S3

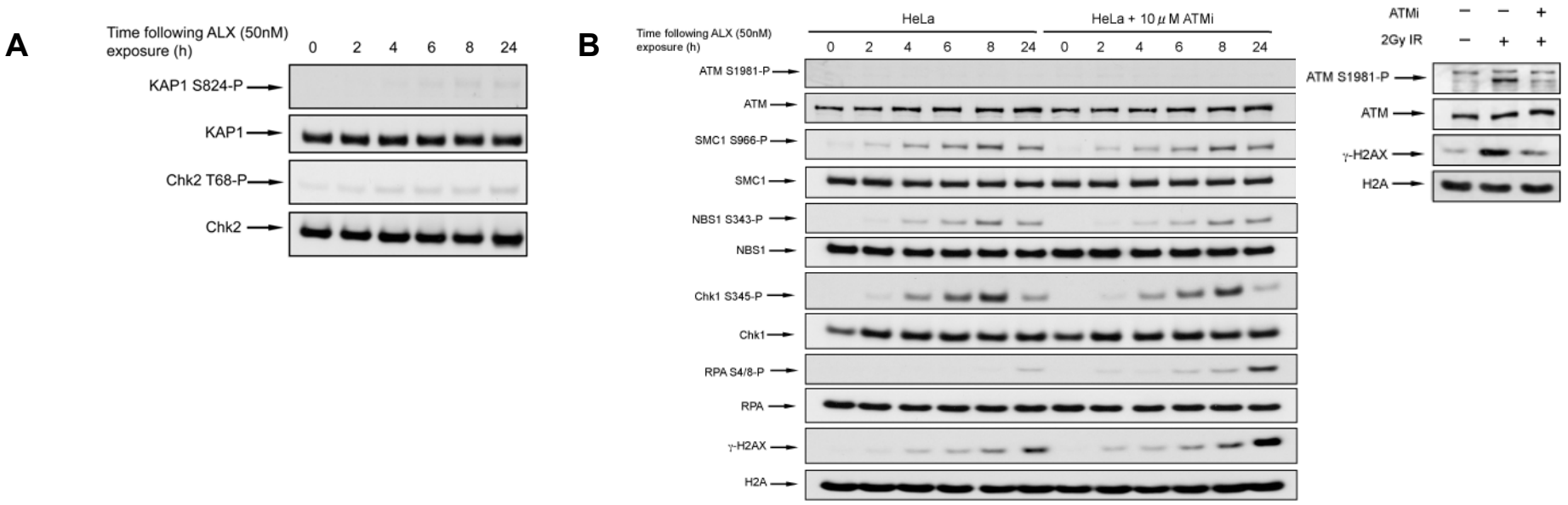
A
Time following ALX (50nM) exposure (h)
0 2 4 6 8 24
KAP1 S824-P
KAP1
Chk2 T68-P
Chk2
B
Time following ALX (50nM) exposure (h)
HeLa
HeLa + 10 μ M ATMi
0 2 4 6 8 24 0 2 4 6 8 24
ATM S1981-P
ATM
SMC1 S966-P
SMC1
NBS1 S343-P
NBS1
Chk1 S345-P
Chk1
RPA S4/8-P
RPA
γ-H2AX
H2A
ATMi − − +
2Gy IR − + +
ATM S1981-P
ATM
γ-H2AX
H2A

Fig. S4

A

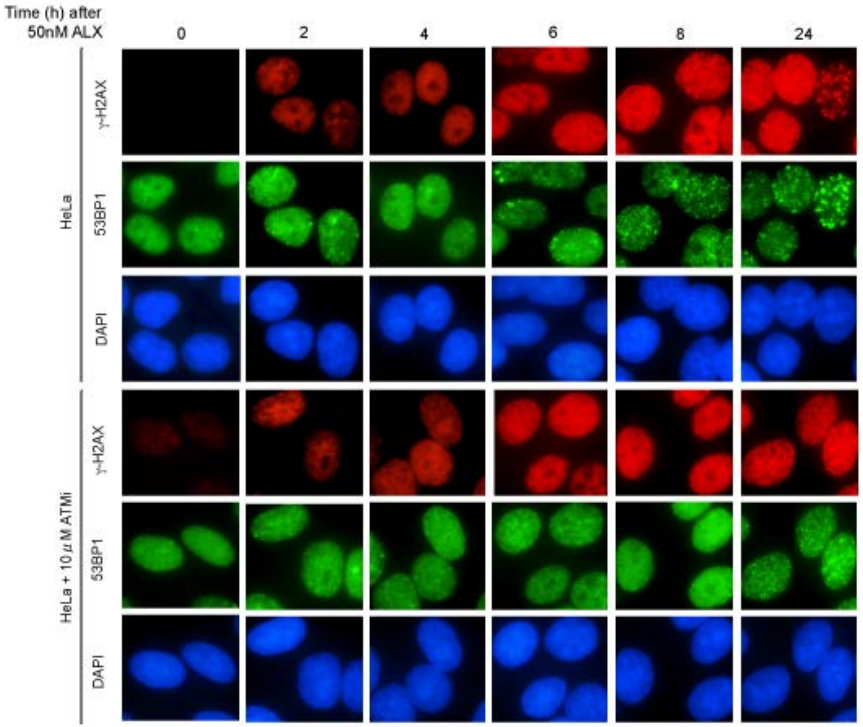
Time (h) after 50nM ALX
0
2
4
6
8
24
HeLa
γ-H2AX
53BP1
DAPI
HeLa + 10 μM ATMi
γ-H2AX
53BP1
DAPI

B

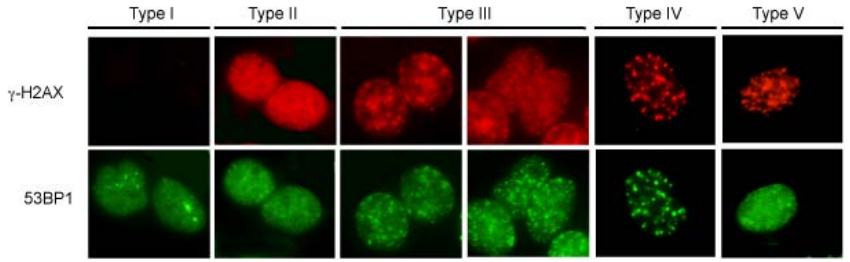
Type I
Type II
Type III
Type IV
Type V
γ-H2AX
53BP1

C

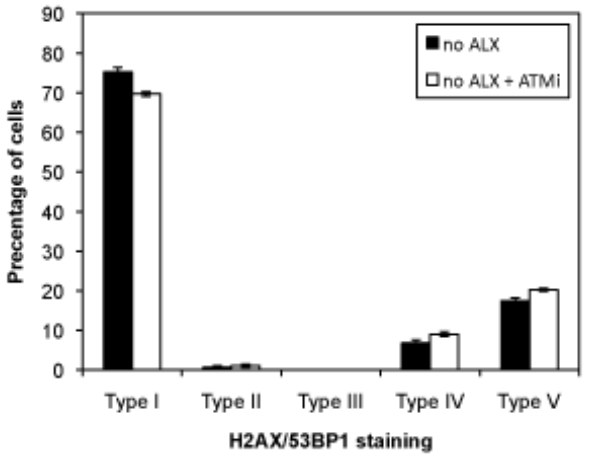
Precentage of cells
no ALX
no ALX + ATMi
Type I
Type II
Type III
Type IV
Type V
H2AX/53BP1 staining

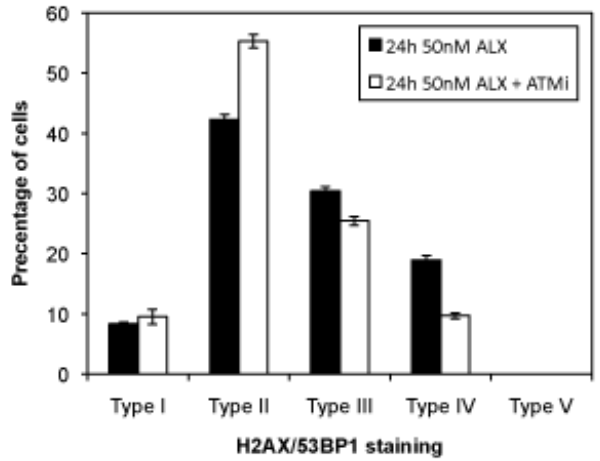
Precentage of cells
24h 50nM ALX
24h 50nM ALX + ATMi
Type I
Type II
Type III
Type IV
Type V
H2AX/53BP1 staining

Fig. S5

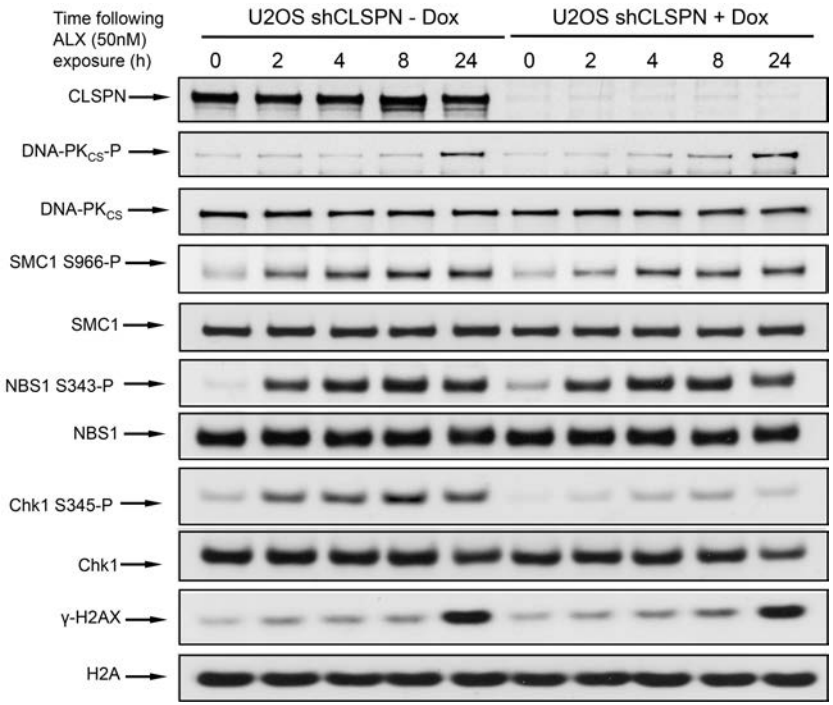
Time following ALX (50nM) exposure (h)
U2OS shCLSPN - Dox
U2OS shCLSPN + Dox
0 2 4 8 24 0 2 4 8 24
CLSPN
DNA-PKcs-P
DNA-PKcs
SMC1 S966-P
SMC1
NBS1 S343-P
NBS1
Chk1 S345-P
Chk1
γ-H2AX
H2A

Fig. S6

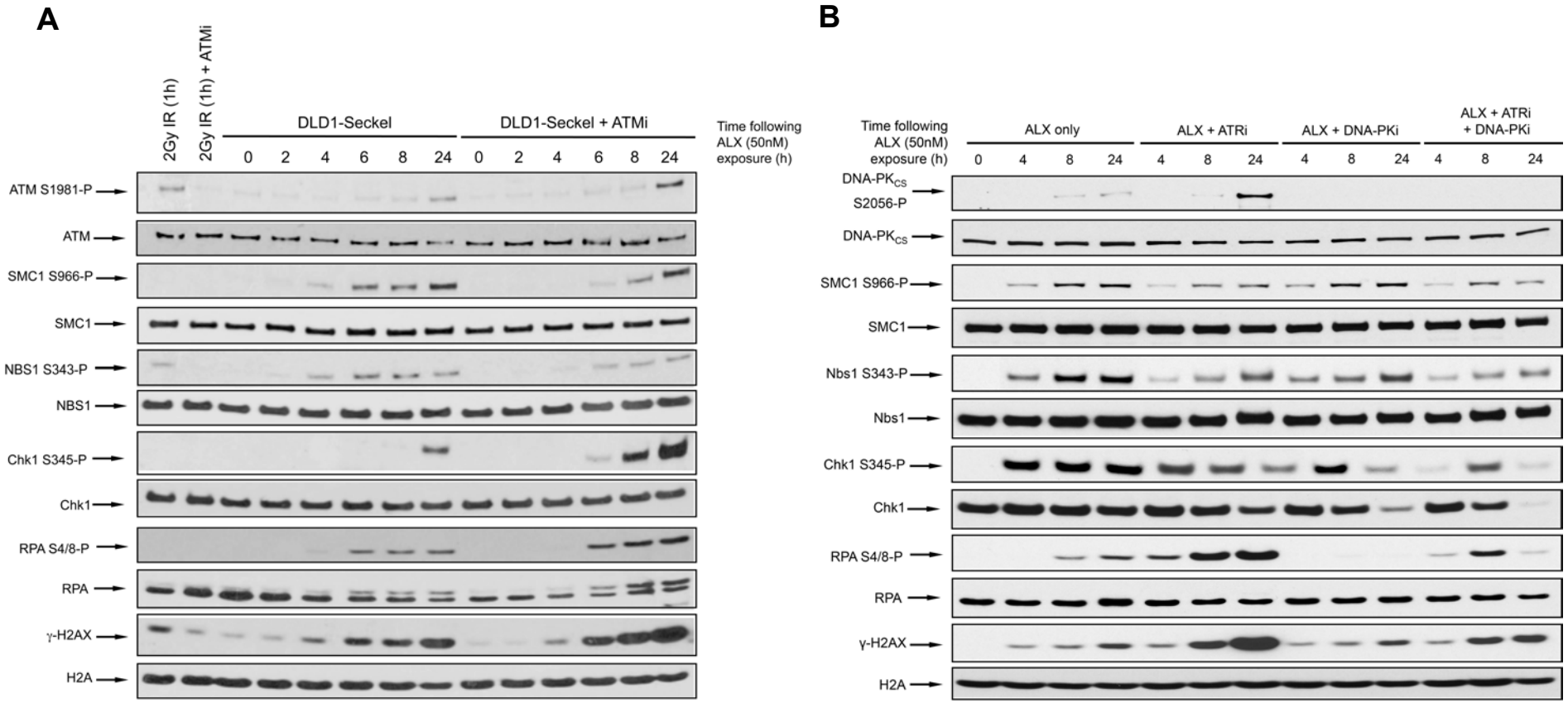
A
2Gy IR (1h)
2Gy IR (1h) + ATMi
DLD1-Seckel
DLD1-Seckel + ATMi
0 2 4 6 8 24 0 2 4 6 8 24
Time following ALX (50nM) exposure (h)
ATM S1981-P
ATM
SMC1 S966-P
SMC1
NBS1 S343-P
NBS1
Chk1 S345-P
Chk1
RPA S4/8-P
RPA
γ-H2AX
H2A
B
Time following ALX (50nM) exposure (h)
ALX only
ALX + ATRi
ALX + DNA-PKi
ALX + ATRi + DNA-PKi
0 4 8 24 4 8 24 4 8 24 4 8 24
DNA-PKcs S2056-P
DNA-PKcs
SMC1 S966-P
SMC1
Nbs1 S343-P
Nbs1
Chk1 S345-P
Chk1
RPA S4/8-P
RPA
γ-H2AX
H2A

Fig. S7

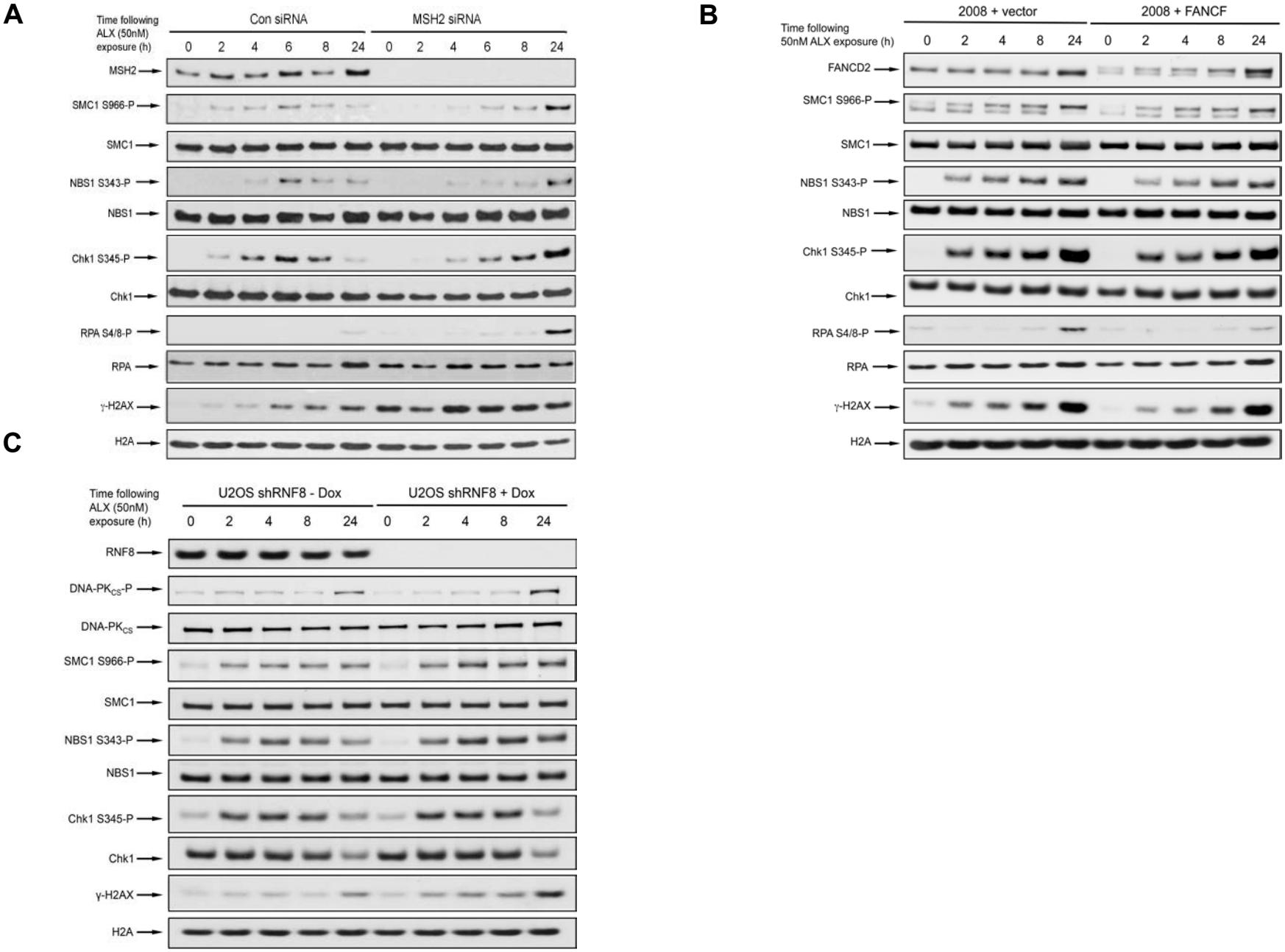
A
Time following ALX (50nM) exposure (h)
Con siRNA
MSH2 siRNA
0 2 4 6 8 24 0 2 4 6 8 24
MSH2
SMC1 S966-P
SMC1
NBS1 S343-P
NBS1
Chk1 S345-P
Chk1
RPA S4/8-P
RPA
γ-H2AX
H2A
B
Time following 50nM ALX exposure (h)
2008 + vector
2008 + FANCF
0 2 4 8 24 0 2 4 8 24
FANCD2
SMC1 S966-P
SMC1
NBS1 S343-P
NBS1
Chk1 S345-P
Chk1
RPA S4/8-P
RPA
γ-H2AX
H2A
C
Time following ALX (50nM) exposure (h)
U2OS shRNF8 - Dox
U2OS shRNF8 + Dox
0 2 4 8 24 0 2 4 8 24
RNF8
DNA-PKcs-P
DNA-PKcs
SMC1 S966-P
SMC1
NBS1 S343-P
NBS1
Chk1 S345-P
Chk1
γ-H2AX
H2A

Fig. S8A

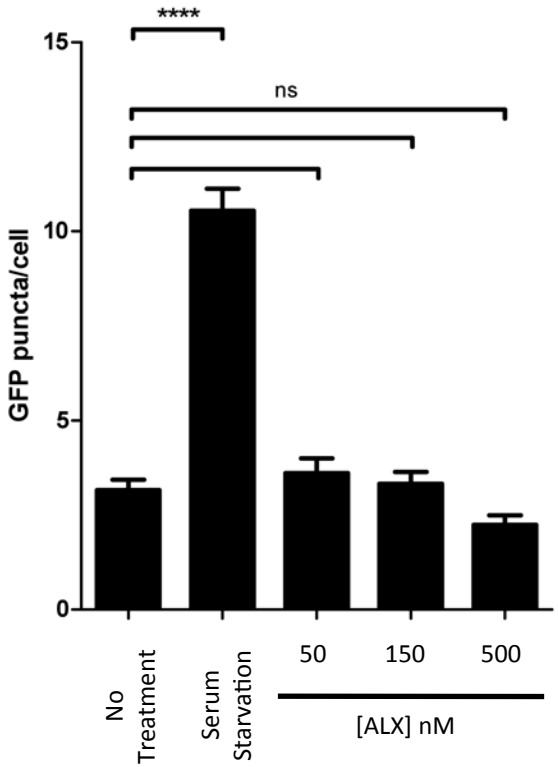
****
ns
15
10
5
0
GFP puncta/cell
No Treatment
Serum Starvation
50
150
500
[ALX] nM

Fig. S8B

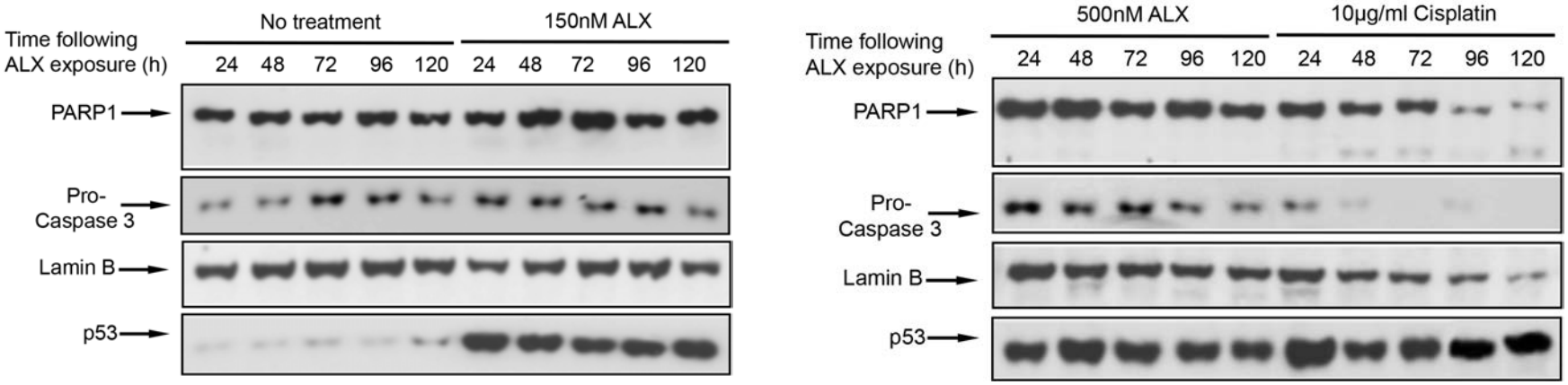
Time following ALX exposure (h)
No treatment
150nM ALX
24 48 72 96 120 24 48 72 96 120
PARP1
Pro-Caspase 3
Lamin B
p53
Time following ALX exposure (h)
500nM ALX
10μg/ml Cisplatin
24 48 72 96 120 24 48 72 96 120
PARP1
Pro-Caspase 3
Lamin B
p53

Fig. S8C

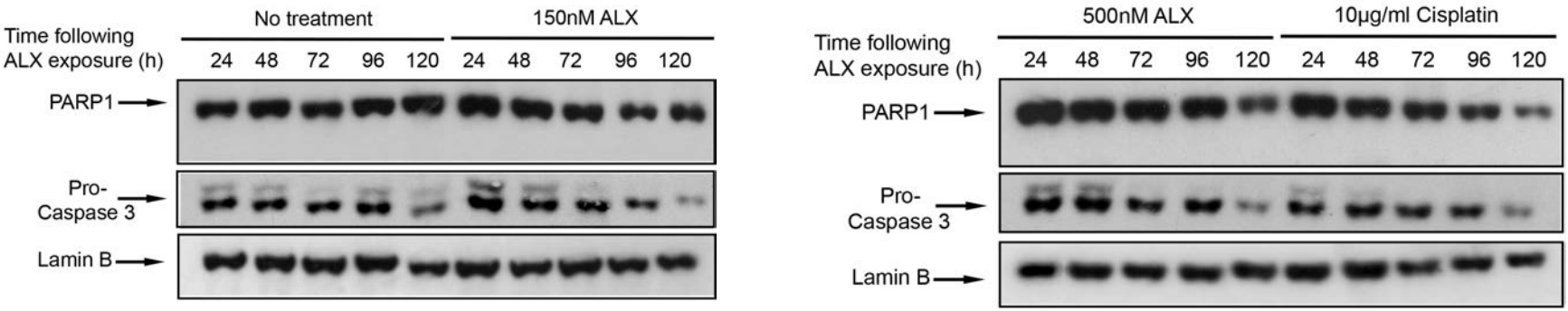
Time following ALX exposure (h)
No treatment
150nM ALX
24 48 72 96 120 24 48 72 96 120
PARP1
Pro-Caspase 3
Lamin B
Time following ALX exposure (h)
500nM ALX
10µg/ml Cisplatin
24 48 72 96 120 24 48 72 96 120
PARP1
Pro-Caspase 3
Lamin B

Fig. S8D

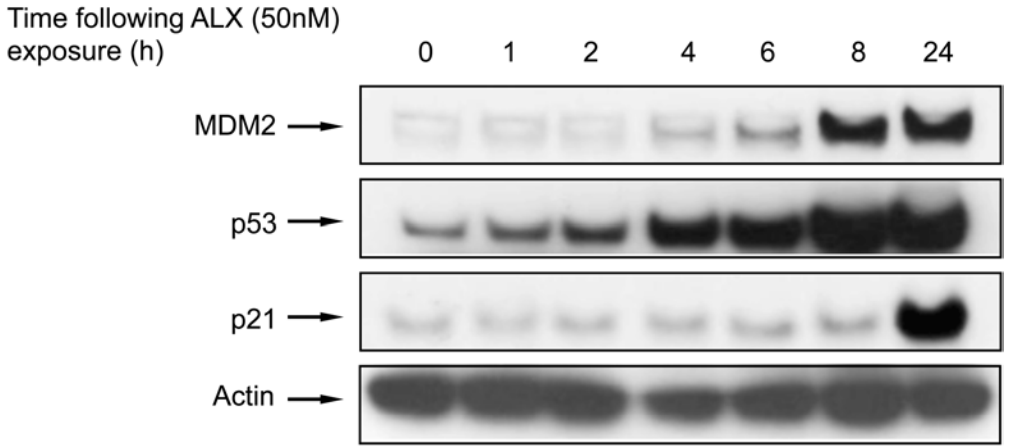
Time following ALX (50nM)
exposure (h)
0
1
2
4
6
8
24
MDM2
p53
p21
Actin

Fig. S9

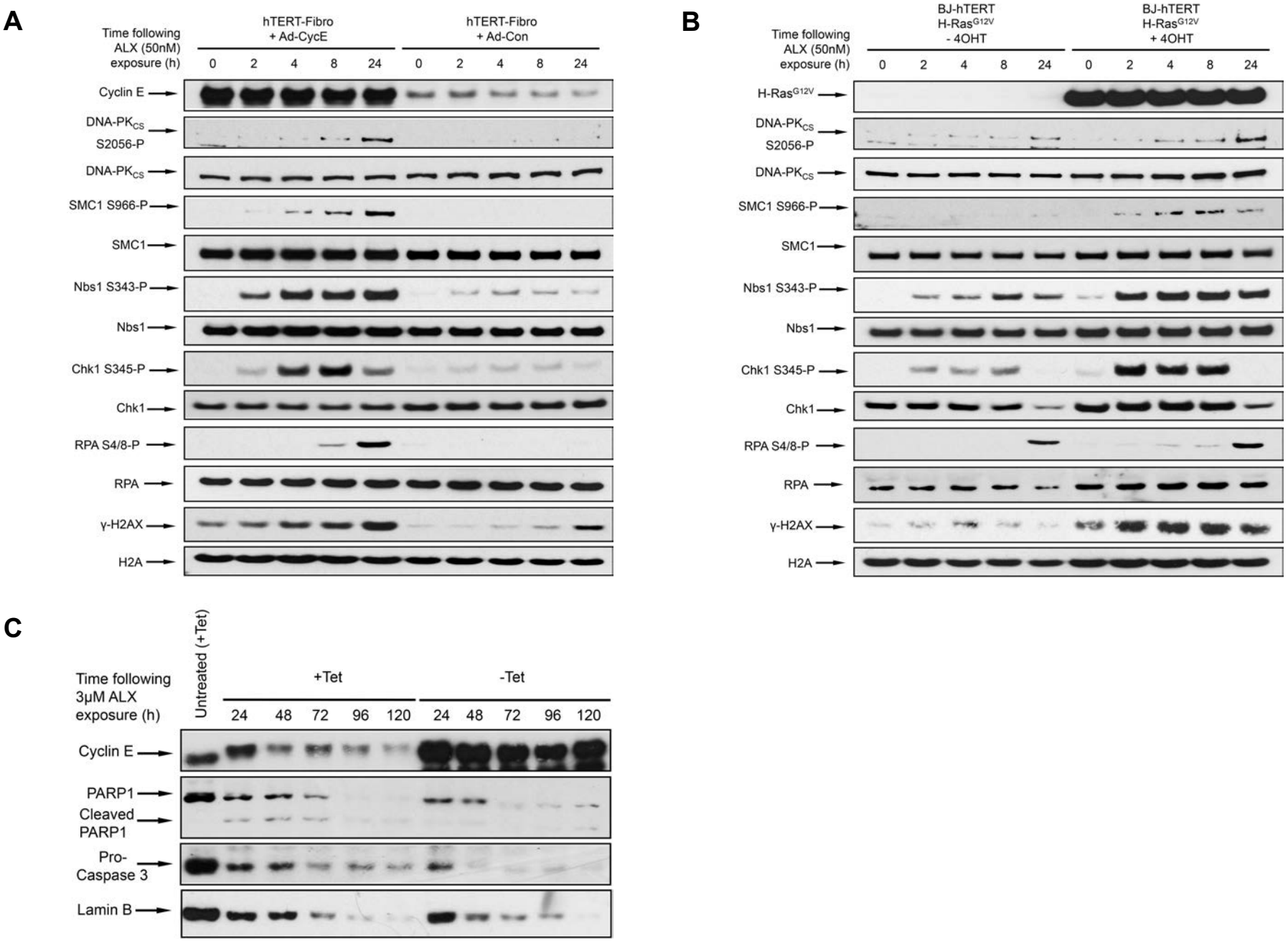
A
Time following ALX (50nM) exposure (h)
hTERT-Fibro + Ad-CycE
hTERT-Fibro + Ad-Con
0 2 4 8 24 0 2 4 8 24
Cyclin E
DNA-PKcs S2056-P
DNA-PKcs
SMC1 S966-P
SMC1
Nbs1 S343-P
Nbs1
Chk1 S345-P
Chk1
RPA S4/8-P
RPA
γ-H2AX
H2A
B
Time following ALX (50nM) exposure (h)
BJ-hTERT H-RasG12V - 4OHT
BJ-hTERT H-RasG12V + 4OHT
0 2 4 8 24 0 2 4 8 24
H-RasG12V
DNA-PKcs S2056-P
DNA-PKcs
SMC1 S966-P
SMC1
Nbs1 S343-P
Nbs1
Chk1 S345-P
Chk1
RPA S4/8-P
RPA
γ-H2AX
H2A
C
Time following 3μM ALX exposure (h)
Untreated (+Tet)
+Tet
-Tet
24 48 72 96 120 24 48 72 96 120
Cyclin E
PARP1
Cleaved PARP1
Pro-Caspase 3
Lamin B

Fig. S10

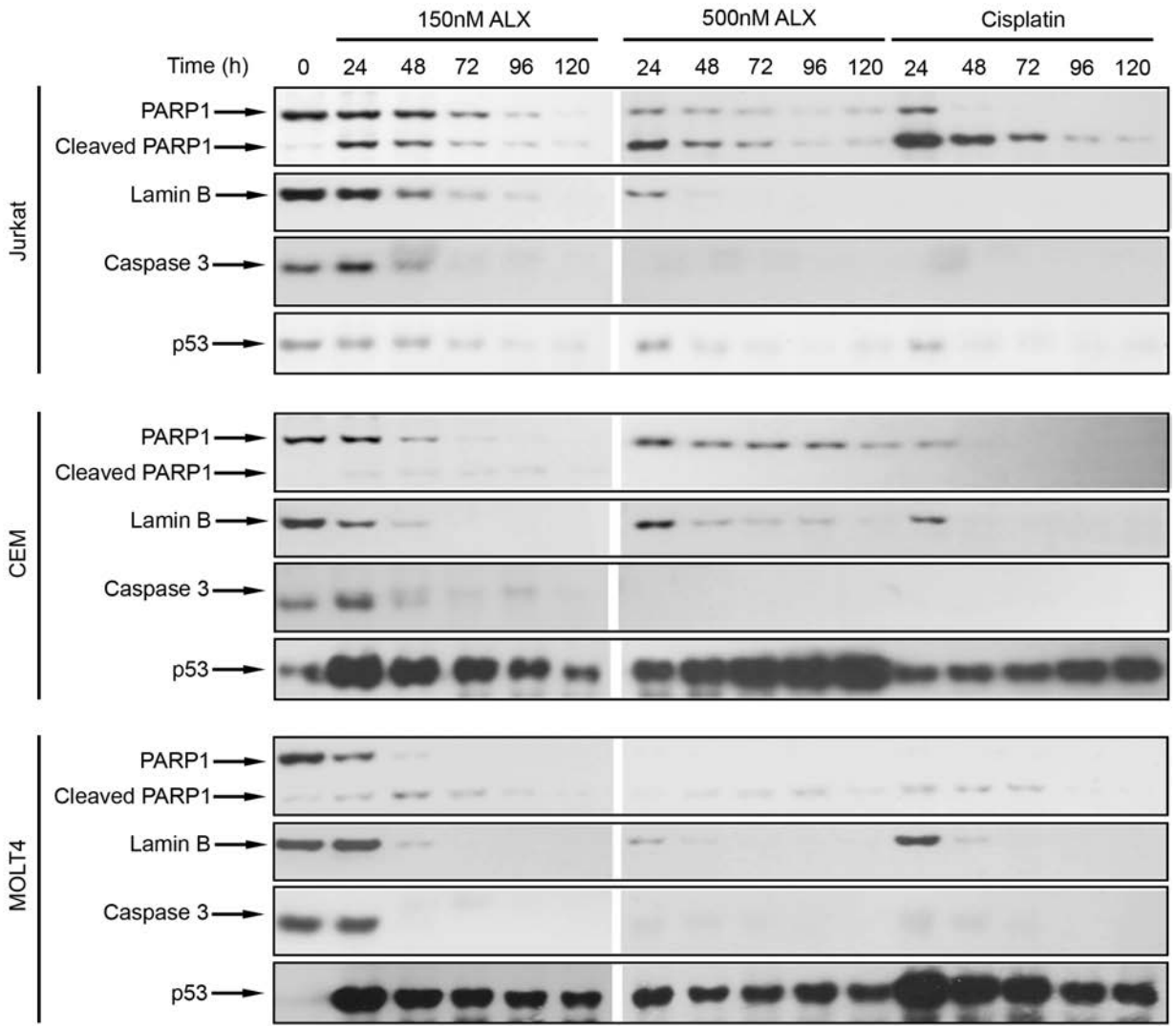
150nM ALX
500nM ALX
Cisplatin
Time (h)
0
24
48
72
96
120
24
48
72
96
120
24
48
72
96
120
Jurkat
CEM
MOLT4
PARP1
Cleaved PARP1
Lamin B
Caspase 3
p53